BLOCKAGE CHARACTERISTICS OF A PLANE COUNTER JET

George Tso-Chi Lin

A DISSERTATION

in

The Faculty of Engineering

Presented in Partial Fulfillment of the Requirements for

the Degree of Master of Engineering at

Sir George Williams University

Montreal, Canada

July, 1972

ABSTRACT

George Tso-Chi Lin

BLOCKAGE CHARACTERISTICS OF A PLANE COUNTER JET

The characteristic of the counter jet has been investigated in the range of Blockage Number, $B = \frac{J}{U^2 H}$, from 0.04 to 0.4. A row of tiny jets (1/32" ϕ) constitutes the counter jet and ensures low Blockage Numbers. It is observed that a definite periodicity was present in the wake flow. Visual observations supplemented hot wire surveys of the wake and confirmed that the scale of mixing increases with increased jet momentum. The Specific Strouhal Number, $S_s = \frac{Jn}{U^3}$, appears to have a value of 0.2 when the body interference effect and the blockage effect were absent.

ACKNOWLEDGEMENTS

The author wishes to thank Dr. A. S. Ramamurthy, and Professor Luc Robillard (Ecole Polytechnique of Montreal) for suggesting the dissertation topic.

Thanks are due to the staff in Ecole Polytechnique of Montreal for the permission to utilize facilities in the Hydraulic Laboratory to make this study possible.

This study is partly supported by N. R. C. under Grant Numbers A4197 and A7608.

TABLE OF CONTENTS

TABLE OF CONTENTS (Cont'd)

LIST OF SYMBOLS

a	total depth of the jet slot
A	total jet area
b	breadth of the jet
B	Blockage Number
d	diameter, jet injection device
D	diameter, cylindrical envelop
F	force
g	acceleration due to gravity
ΔH	manometer reading, main flow
Δh	manometer reading, jet flow
H	total depth of the main flow
J	kinematic jet momentum per unit breadth
K	velocity ratio, V/U or $\overline{V}/\overline{U}$
M	total jet momentum per unit breadth
M'	total jet momentum
n	frequency
p_{tot}	total pressure
Pst	static pressure
Q_j	rate of flow, jet flow
Q_m	rate of flow, main flow
R	reading of the total head tube
R_s	reading of the static head tube
R	Reynolds Number
R_s	Specific Reynolds Number (also jet Reynolds number)
r	radius

S	Strouhal Number
S_s	Specific Strouhal Number (also jet Strouhal number)
T	time
U	main flow velocity, local
$\overline{U}$	main flow velocity, mean
V	initial jet velocity, local
$\overline{V}$	initial jet velocity, mean
v	local jet flow velocity
w	width of the wake
wt	weight
ρ	density
μ	viscosity
ν	kinematic viscosity
θ	inclination

LIST OF TABLES

LIST OF FIGURES

LIST OF FIGURES

BLOCKAGE CHARACTERISTICS OF A FLUID COUNTER JET

INTRODUCTION

The study of penetrating a plane jet into a counter flow by Robillard [1] has revealed that the instability mentioned in Hopkins' work [2] turned out to be a periodic oscillation of jet sheet which leads to vortex shedding in a manner similar to the Karman vortex street. The vortex shedding mechanism was assumed earlier [1] to be unaffected by the jet injection device. This behaviour was apparent when the depth of the injection slot was small relative to the width of the near wake where the vortices formed.

In this thesis, the flow characteristics of the counter jet is studied for a wider range of fluid and geometric parameters which are expected to influence the jet instability. Included in this study is the important concept of blockage caused by the interference of the lateral boundaries.

Wake surveys were conducted to investigate solid body interference with jet oscillations, which has revealed some interesting modulation effects in the wake oscillation records.

This study will ha-e significant bearings on:

1) thermal pollution problems related to coolant water injection in rivers against the main current for better mixing, e.g. neuclear power plant wastes;

(2) jet vehicles cruising with a leeward wing;

(3) vibration induced by the reversing jet thrust applied during landing of jet vehicles.

PREVIOUS WORK

The formation of vortices behind a cylindrical body immersed in a running stream has long been known as the Karman vortex street. The shedding of these vortices was later investigated by Strouhal [3] whose experiments had led to an empirical correlation, a dimensionless Strouhal number $S = \frac{n\,d}{U}$. Here n is the frequency of the vortex shedding, d the diameter of the cylinder, and U the stream velocity.

This Strouhal number depends uniquely on the Reynolds number $R = \frac{\rho U d}{\mu}$, where ρ is the density of the fluid, and μ the viscosity.

Subsequent measurements performed by Roshko [4] revealed that at nigh Reynolds number ($R > 1200$) the Strouhal number remains approximately constant at $S = 0.21$. The experimental points which were obtained by Roshko with cylinders of different diameter d and at various velocities U arrange themselves well on a single curve (Figure 1).

The dimensionless "Specific Strouhal Number", $S_s = \frac{J\,n}{U^3}$, adopted in this study accords with Robillard's [1] approach, where J is the initial kinematic momentum of the jet per unit breadth. This specific Strouhal number is developed from the parameter that Rao [5] has applied in his investigation of the problem of an axisymmetrical jet in a counter flow. He characterized the jet by a single parameter, the "initial kinematic momentum", $J' = \pi r^2 V^2$, r being the radius of the orifice, and V the initial jet velocity. He also used the physical quantity $J'^{1/2}/U$ as a characteristic length in his dimensional analysis.

For a plane jet in a stationary type of flow the "initial kinematic momentum per unit breadth" should be $J = aV^2$, a being the depth of the slot† if the jet opening is rectangular as the one used in the preliminary test [6]. If one applies J/U^2 as a characteristic length in the dimensionless Strouhal number $S = \frac{n\,d}{U}$, a new dimensionless number will be expressed in terms of J instead of d. This new expression is given a name "Specific Strouhal Number", S_s, and

$$S_s = \frac{n}{U}\frac{J}{U^2} = \frac{n\,a}{U}\frac{V^2}{U^2} = \frac{n\,a}{U}K^2 \quad \ldots\ldots\ldots\ldots\ldots (1)$$

where K is the velocity ratio V/U.

If the same characteristic length is applied in the dimensionless Reynolds number, $R = \frac{\rho U d}{\mu}$, one may obtain an expression for the new dimensionless number which is given a name "Specific Reynolds Number", R_s, and

$$R_s = \frac{\rho J}{\mu U} = \frac{\rho U a}{\mu}\frac{V^2}{U^2} = \frac{\rho U a}{\mu}K^2 \quad \ldots\ldots\ldots\ldots\ldots (2)$$

In fact the initial kinematic jet momentum per unit breadth, $J = aV^2$, is a crude representation where in real flow conditions the contraction effect and the non-uniform velocity profile of the jet flow prevent the direct application of this relation. For this reason, the use of parameter J instead of a and V would be advantageous, if J could be measured directly. It is especially true in the present case as the injection device had a row of tiny round holes along the tube instead of a rectangular slot (Figure 4). Note that the former is easier to fabricate. To this end, a sentitive balance has been designed to measure jet momentum directly, and experimental data obtained have been verified to be consistent.

---

† A 1/16" x 10" slot was provided on the injection device.

The experiments performed by Colin [7] on a wall jet in a counter flow showed that a strong stationary eddy was produced by the rolling up of the jet napple. In a stable flow, it is conceivable that a wall jet as such is only the upper half of a free plane jet in a counterflow, where the wall boundary may be considered as the centre line of the jet. The flow pattern for a wall jet in counterflow as shown in Colin's paper may be transformed to a flow pattern as for a counterjet as the problem at hand [8]. Figure 2 shows the transformed flow pattern which is symmetrical with a pair of vortices rolling in opposite direction.

Since the jet centre line velocity decreases in proportion to a power of the distance x [9,10], the stagnation point as shown in Figure 2 will occur at a distance from the jet discharge, where the jet centre-line velocity equals and opposites the velocity of the main stream. This distance is surely affected by the magnitude of the jet momentum and the main stream momentum, which in turn affects the height of the envelope created by the separating streamline, on both sides of the jet centre-line.

This argument has led to the adoption of the dimensionless Blockage Number, B, and

$$B = \frac{J}{U^2 H} \qquad \ldots\ldots\ldots\ldots\ldots\ldots\ldots\ldots \quad (3)$$

If, again, the initial kinematic momentum per unit breadth is expressed as $J = aV^2$, a being the total depth of the jet slot, then

$$B = \frac{a}{H}\frac{V^2}{U^2} = \frac{\rho Q_j V}{\rho Q_m U} \qquad \ldots\ldots\ldots\ldots\ldots\ldots\ldots \quad (3a)$$

which is a ratio of momentum per unit breadth of the jet flow to that of the main flow in the same fluid medium.

EXPERIMENTAL EQUIPMENT AND TEST PROCEDURE

Water Tunnel

The water tunnel used for this study consisted of three sections, i.e. supply section, test section and discharge section. Figure 3 shows the general layout.

The inlet of the supply section contained a metering elbow, to which a mercury manometer was connected to measure the rate of flow, Q_m , of the main stream. Before leading the flow into the supply tank, a diffuser and disc deflector were employed to slow down the velocity. Through various perforated plates, meshes and rubberized hairs, the flow was then channelled to the test section by a pair of bi-dimensional converging plates.

The test section proper was an open channel. It was 10" wide, 72" high and 96" long. It stood vertically with a reinforced 1" plexiglass panel on each sidewall.

A tape ruler was affixed vertically on the sidewall 10" downstream from the centre of hole where the injection device was installed. By injecting dye in the jet flow, the width of the jet wake was qualitatively measured.

The free surface level was adjustable by raising or lowering a weir which was installed in the discharge section. The discharge section was a simple reservoir which maintained a constant rate of discharge with less disturbance to the uniformity of flow inside the test section.

A carriage was installed on top of the test section. A probe supporting fixture rode on it. It allowed the probe to be placed at any desired location along X axis (parallel to the main flow), and with a vernior and a sliding rod, it allowed the probe to be adjested at any elevation along the Z axis (Figure 8).

Injection Device

The injection device employed in this study was a cylindrical tube with a nominal inner diameter of ½". The outside diameter of the tube was 0.539". A row of 80 holes of 1/32" dismeter each was drilled along the tube, evenly spaced 1/8" apart (Figure 4). The effective length (or breadth) of the jet was 10". The tube was installed transversely at the centre of the test section. With a boss bounded to the outer surface of each sidewall and a series of sleeve, seal and retainer, the tubular injection device could be adjusted radially to obtain any desired jet orientation.

Two high pressure hoses of 1" diameter of the same length were connected to the injection device, one at each end, to ensure even inlet from each end of the tube, forming an even discharge of jet along the whole breadth (Figure 4).

The 80 hole arrangement was considered to be the maximum, limited by the cross sectional area of the tube.

The water supply of the injection device was provided from two systems: one was supplied by a one HP water pump, and the other by a large water

reservoir located about 30 feet above the elevation of the jet. The latter provided a more steady pressure of the jet flow within its capable range, for precision calibrations such as jet momentum measurement.

Two separate globe valves, one in each system, controlled the rate of jet flow. These two systems were interconnected by a 1½" Tee, where a dye fluid discharge line was connected.

The dye reservoir of a 2 gallon capacity was precharged with compressed air when in use. Cocks were installed to control the rate of discharge of the dye fluid and to regulate the internal air pressure. Leading from 1½" Tee, a fine mesh filter was installed to prevent any sizeable dirts from entering the injection system. This filter was periodically replaced. At about 36" downstream of the filter, a ½" diameter metering orifice was installed. This orifice was used to calibrate the rate of flow of the jet, Q_j , by connecting the cavity on each side of the orifice to a manometer. The 36" length of the pipe was considered necessary and sufficient to ensure a steady flow before entering the orifice section.

The fluid used in the manometer was carbon tetrachloride or mercury depending on the range of Q_j to be measured. The two 1" high pressure hoses were connected to the downstream of the orifice through another 36" long pipe, and 1½" Tee and reducers.

Figure 4 gives a sketch of this jet injection system.

Momentum Calibration Set-Up

The total momentum of a jet is

$$M' = \rho Q_j V \qquad \ldots\ldots\ldots\ldots\ldots\ldots \quad (4)$$

V being the initial jet velocity. Presumably the jet velocity is not far from uniform in the inlet section.

In reality, however, except at low Reynolds numbers based on jet velocity and the width of the jet, the jet always becomes completely turbulent at a short distance from the point of discharge. Because of friction developed on the periphery, the emerging jet becomes partially mixed with the surrounding fluid at rest.† Particles of fluid from the surrounding are carried away by the jet so that the mass flow increases in the downstream direction. Consequently the jet spreads out and its velocity decreases, but the total momentum remains constant, independent of the distance x from the orifice. The total momentum of a jet per unit breadth

$$M = \frac{M'}{b} = \rho \int_{\infty} v^2 dz = \text{constant}^{*} \qquad \ldots\ldots\ldots \quad (5)$$

v being local jet velocity along the X-direction with respect to a specific z.

This equation is valid for both laminar and turbulent free jets, and was discussed in depth by Schlichting [10].

---

† Assume that the main flow is stationary.

* Assume that the jet velocity is not far from uniform along the breadth.

Since measuring the local velocity and its distribution are very time consuming, a direct measuring method of the total jet momentum is a practical solution†.

When a jet impinges on a solid plate at a normal (90^{o}) direction, the fluid spreads along the plate. It imposes a steady force on the plate, equivalent to the total momentum of the jet, provided that the plate covers the complete area of the jet flow. While jet is immersed in the same type of fluid, particles in the surrounding being carried away by the jet absorb partly the jet momentum. When the plate is large enough to cover all the moving particles, the total momentum acting on the plate shall remain constant.

The balance (Figure 6) designed for this study consisted of a "T" shape arm made from 1/8" aluminum plate. The horizontal arm, from fulcrum to pivot, was 10" and the vertical leg, from fulcrum to the centre line of the jet impinging plate was 20", which maintained a 2:1 ratio for easy calculation. A disc for placing counter weights was hung at one end of the arm, and a small adjustable rider was attached to the other arm to compensate any initial unbalanced conditions. The jet impinging plate was a plain 1/8" plexiglass 3" wide and 12" long, attached to the vertical leg with screws. A dial was attached to the platform to guide the level position.

---

† Similar apparatus was used to measure impinging force of air jets, Ref. ASCE Journal, Hyd. Div. November 1970, P 2234

The balance was supported rigidly by an aluminum frame and platform. On the platform a slot was provided to guide the "T" arm from over swinging.

A pair of fixtures, installed 13" apart were mounted on the platform to support the injection device. The position of the injection device was adjustable both vertically and horizontally by simple mechanisms built in the fixture, and the long slots on the platform. The slot were about 5" long which allow an ample adjustment horizontally.

The test tank was 30" x 30", and 24" high. A weir was installed inside the tank near the outlet port, to maintain a constant water level of 13". A 9" x 14" baffle plate was installed approximately 3¼" behind the impinging plate of the balance, to minimise eddies which may induce errors to the jet momentum reading. The whole test tank including weir and baffle plate were made of transparent plexiglass so that all flow conditions when desired, could be observed easily by adding dye fluid in the jet stream.

A total head tube (1/20" O.D., 1/40" I.D.) was used to measure the velocity distribution in the down stream of the jet. This tiny total head tube was connected to a simple glass capillary tube having 1-millimeter scale increments. The capillary tube was filled with water and purged thoroughly to bleed any air bubbles and contaminations out of the system to assure accuracy. The static head was deducted from the total head to arrive at the velocity head.

A vernier unit, Lory Type A, capable of reading one-tenth of a millimeter, was mounted vertically to the test tank structure. The total

head tube was secured on the sliding shaft of the vernier unit, by clamping blocks so that the tip of the total head tube aligned with the front surface of the jet impinging plate in its upright position. The vertical position of the total head tube was adjustable by means of the vernier unit throughout its complete range.

The glass capillary tube was placed at a 10 to 2 inclination to attain high accuracy. It was affixed on the test tank so that static pressure reading could be properly maintained.

The complete balance and the baffle plate were removed when measuring velocity distribution of the jet profile. A 2" rubberized hair pad was placed in front of the weir, to absorb any possible bouncing effect of the jet flow in the downstream region.

The force on the plate was purely a function of the jet discharge (and hence its momentum for a given jet injection tube). It does not vary either with the depth of immersion (static head change) or the location of the jet impinging plate from the jet injection tube. This supports the invariance of jet momentum in the downstream direction which was taken for granted in the beginning.

Figures 5 and 6 illustrate the overall set up of the balance, and Figure 7 the total head tube installation. Appendix 1 gives the detail of the balance.

Frequency Measurement

A hot film anemometer was mounted on a vernier unit which, moving with the fixture as a whole, rode on the carriage on top of the test section, allowing the anemometer to move in all directions. The vernier unit was capable of reading one thousandth of a foot.

The support of the hot film anemometer permitted the hot film to be oriented in a desired direction.

Through the electronic set-up as explained in Figure 12, signals picked up by the anemometer were displayed on strip charts for time series study. Frequencies of vortex shedding are determined from the strip charts when the shedding is regular.

For low shedding frequencies, visual counting method was employed by injecting dye fluid into the jet flow and counting the shedding with a chronometer.

When the shedding was slightly irregular the signals were stored on the magnetic tape for further analysis on the B & K wave analyzer.

Main Flow Velocity Measurement

Three different methods were employed to measure the main flow velocity: (a) By determining the vortex shedding frequency in the wake behind a small cylindrical body (the existing injection device) and then calculating the flow velocity through the Strouhal number - Reynolds number relation (Figure 1); (b) By using a Mini-flowmeter Counter Unit (Type

176/2 MK2) and a calibrated Micro Propeller to measure flow velocity directly at a specific point; (c) By a Prandtl pitot tube and an inclined manometer. Since the use of Prandtl pitot tube was very time consuming, methods (a) and (b) were adopted in most cases during the experiment.

The rate of main flow, Q_m , was calibrated with a manometer connected to the ports at the inner and outer radii of the bend of the elbow leading to the water tunnel supply tank. Figure 8 shows the calibration curve of the rate of main flow versus manometer reading, $\Delta H_{(Hg)}$.

Mean velocity, $\overline{U}$, of the main flow is then calculated from the curve, such that

$$\overline{U} = \frac{Q_m}{b\,H} \qquad \ldots\ldots\ldots\ldots\ldots\ldots\ldots\ldots (6)$$

b being the breadth and H the height of the main flow inside the test section. Since velocity profiles across the test section were found non-uniform due to turbulence, the mean velocity $\overline{U}$ was used as reference only.

The term "local main flow velocity U" denotes the main flow velocity along the X-direction in the vicinity of the centre line of the jet injection device at a specific location of y (Figure 8).

On method (a), vortex shedding signals were picked up by a probe (hot film anemometer), which were then recorded on strip charts. The position of the probe was at the centre of the test section (y = 0). When the frequency n is known the corresponding local main flow velocity can be obtained from the equation:

$$U = \frac{n\,d}{S} = 0.214\ n \quad \text{ft/sec} \qquad \ldots\ldots\ldots\ldots (7)$$

On method (b), a micro propeller was submerged in the test section, 6" ahead of the injection device at y = 0. Turning speeds of the micro propeller give the corresponding flow velocities through a calibration chart. To ensure accuracy this calibration chart has been verified through towing tests.

The main flow velocities obtained by both methods were reasonably in agreement. However, due to fluctuation of the supply, to maintain a constant main flow velocity has been found quite difficult.

Table 1 shows all data verified by the three different methods.

Rate of Flow Metering

The ½" diameter metering orifice as explained earlier was the key instrument to determine rate of the jet flow. The orifice was calibrated by direct measuring method. A container of 20 gallon capacity, a weighing scale, and a chronometer were used to measure the exact time required to collect a set weight of water. Results are later converted in terms of volume per unit of time, ft^3/sec, versus corresponding manometer settings.

Several measurements were made for each manometer setting and the average value was adopted for accuracy. Table 2 tabulates the calibration results, and Figure 10 plots the relations, Δh vs. Q_j, Δh vs. $\bar{V}$, and Q_j vs. J.

Jet Momentum Measurement

The test tank as shown in Figure 5 was rigidly supported and levelled up on top of a concrete stand. The two 1" rubber hoses leading from the jet system were connected to the 0.539" tubular injection device which is the same injection device employed throughout this study.

The orientation of the jet was checked by injecting water into the system and discharging the jet stream in air. Adjustments were made to level the stream to the centre line of the jet impinging plate of the balance and to maintain an even distance between the injection device and the jet impinging plate.

Before conducting measurements, the complete jet system was purged to remove any air bubbles which might be trapped in the calibrated orifice installation, the manometer and the connecting hoses. Dye fluid was injected in the system to observe the flow pattern inside the tank. Plates 1 and 2 are photos taken during the experiment, which show even flow along the upper half and the lower half of the impinging plate.

One can reasonably assume that the flow discharged from the test tank, running over the weir had no significant influence to the jet momentum impinging on the plate.

The experiment was conducted inside a room free from air drifting. Masses (weights) of various values, down to a 0.05 of a gram were used for the measurement.

Three different jet to plate distances (the distance between the jet exit and the front surface of the jet impinging plate) were chosen. At a distance of 1 3/8" and 2 1/4", the balance was unstable. It could hardly establish a definite value; either the jet impinging plate was swinging away from the jet exit, or swinging all the way toward the jet exit, when a slight weight is added or removed. The third distance of 3 1/8" or more was found satisfactory. Same measurements could be repeated with an accuracy of ±0.1 gram at low flow rates. Table 3 tabulates all the data measured and Figure 11 shows the plot.

It is worth noting that although there was a poor stability at a shorter jet-to-plate distance, the mean readings obtained as plotted in Figure 11 still present a fairly consistent trend.

As a matter of interest, a few readings were taken when the test tank was empty (i.e. jet being discharged in air). Forces measured were consistently lower than that measured with the jet immersed in water. The surface tension of the water stream while in air, could have reduced the effective jet momentum acting on the jet impinging plate.

Electronic Instrumentation

Figure 12 shows the electronic instrumentation system employed for this study. The dotted line indicates the suggested procedure for further analysis of data by digital methods. The following instruments were used during the investigation:

(1) Constant Temperature Anemometer - DISA Type 55D01 including Probe (Hot Film Unit) 55A58.

(2) Attenuator (Amplifier) - DISA

(3) Low Pass Filter

(4) Sanborn Recorder

(5) Oscilloscopt - Hewlett Parkard Model 120B.

(6) RMS (Auxiliary Unit) - DISA Type 55D25.

(7) Tape Recorder - B & K Type 7001.

(8) Analyser - B & K.

DIMENSIONAL ANALYSIS

Specific Strouhal Number

The physical quantities which determine the shedding frequency of a counter jet include the main flow velocity U, the jet stream velocity V, the size of the jet discharge A, and the density of the flow media, ρ. As the jet stream velocity is not uniform across the jet exit, it is much convenient to represent the jet in terms of momentum per unit breadth M, instead of V, A, and ρ. The jet momentum is measurable in terms of force, and the initial kinematic jet momentum per unit breadth

$$J = \frac{M}{\rho} \quad ft^3/sec^2 \quad \ldots\ldots\ldots\ldots\ldots\ldots (8)$$

We now determine the dimensionless combination of quantities in the form

$$\Pi_1 = \pi_1[M\ U^{\beta} n^{\gamma} \rho^{\delta}]$$

Let F denotes force, L length, and T time. Then the dimensionless combination will be

$$\pi_1[\ M^{\alpha} U^{\beta} n^{\gamma} \rho^{\delta}\ ] = F^{o}\ L^{o}\ T^{o}$$

Assume $\alpha = 1$, we have

$$\pi_1 [M U^{\beta} n^{\gamma} \rho^{\delta}] = (\frac{F}{L}) (\frac{L}{T})^{\beta} (\frac{1}{T})^{\gamma} (\frac{FT2}{L^4})^{\delta} = F^{o} L^{o} T^{o}$$

and

F: $1 + \delta = 0$

L: $-1 + \beta - 4\delta = 0$

T: $-\beta - \gamma + 2\delta = 0$

The solution of the above is:

$$\delta = -1, \quad \beta = -3, \quad \gamma = 1.$$

The unique dimensionless combination of the four quantities M, U, n, and ρ is:

$$\Pi_1 = \frac{M n}{\rho U^3} = \frac{J n}{U^3}.$$

Π_1 is denoted as Specific Strouhal Number S_s.

Specific Reynolds Number

The physical quantities which determine the flow in counterjet system are: the free stream velocity U, a characteristic linear dimension of the jet in terms of kinematic momentum per unit breadth J (for instance, J/U^2), the density ρ, and the dynamic viscosity μ. We now determine the dimensionless combination of quantities in the form

$$\Pi_2 = \pi_2 [J^{\alpha} U^{\beta} \rho^{\gamma} \mu^{\delta}] = F^{o} L^{o} T^{o}$$

Assume $\alpha = 1$, to obtain dimensionless combination

$$\pi_2 [J^{\alpha} U^{\beta} \rho^{\gamma} \mu^{\delta}] = (\frac{L^3}{T^2}) (\frac{L}{T})^{\beta} (\frac{FT^2}{L^4})^{\gamma} (\frac{FT}{L^2})^{\delta} = F^{o} L^{o} T^{o}$$

and

F: $\gamma + \delta = 0$

L: $3 + \beta - 4\gamma - 2\delta = 0$

T: $-2 - \beta + 2\gamma + \delta = 0.$

From the above relations, we have the solution that,

$$\gamma = 1, \quad \delta = 1, \quad \beta = -1.$$

The unique dimensionless combination of the four quantities J, U, ρ, and μ is

$$\Pi_2 = \frac{J\rho}{\mu U} = \frac{J}{\nu U}$$

Π_2 is denoted as Specific Reynolds Number R_s.

Blockage Number

The blockage number in the present study consists of three physical quantities: i.e. the free stream velocity U, the kinematic jet momentum per unit breadth J, and the depth of the free stream H. The dimensionless combination will be:

$$\Pi_3 = \pi_3 [J^\alpha U^\beta H^\gamma] = (\frac{L3}{T2})^\alpha (\frac{L}{T})^\beta (L)^\gamma = F^o L^o T^o.$$

As $\alpha = 1$, it can be easily seen that $\beta = -2$ and $\gamma = -1$. The unique dimensionless combination of the three quantities J, U, and H is

$$\Pi_3 = \frac{J}{U^2 H}$$

Π_3 is denoted as Blockage Number B.

DISCUSSION OF RESULTS

Jet Momentum

The previous sections have explained generally how the jet momentum was measured, and this data is presented in Tables 2 and 3. The following observations and analyses have been carried out to provide some cross checks on the computations of jet momentum.

(A) By introducing a dye into jet system, the jet flow pattern was closely observed. This visual observation of the flow pattern proved that the force reading measured by the balance is the total impinging force caused by the complete jet stream. The jet left the plate in a tangential direction to the plate after impact (Figure 25). At a jet-to-plate distance of 3 1/8" the stream hitting on the plate was estimated to be about ¼" thick. The mixing zones, above and under the jet sheet (as indicated by the gradually vanishing color) extended symmetrically about the axis of holes to a width of about 1½". The jet impinging plate was 3" wide and as such, one can be sure that the complete jet stream is totally covered by the plate.

(B) The velocity profile of the jet flow was obtained by using a tiny total head tube as explained earlier. The profile was measured under a rate of flow Q_j at 0.0081 ft^3/sec. The distance between the total head tube tip and the jet exit was 3 1/8". Table 4 tabulates the measured data and Figure 13 shows the complete profile.

From Eqn. (5), for discrete measurement, one may calculate the total jet momentum (Figure 13a) by:

$$F = M\,b = \rho\int_{\infty} v^2\, b\, dz = \rho\sum_{z} v^2\, b\, \Delta z \quad \ldots\ldots\ldots\ldots (9)$$

The breadth b of the injection device is 10 inches.

From Bernoulli equation, we have

$$\frac{p_{tot} - p_{st}}{\gamma} = \frac{v^2}{2g} \quad \ldots\ldots\ldots\ldots\ldots\ldots (10)$$

In Table 4 θ denotes the inclination of the capillary tube. Hence, denoting the readings of the total head tube and the static head tube as R and R_s, one can write:

$$\begin{aligned} F &= \rho \int_{\infty} 2g\,(R - R_s)\,\mathrm{Sin}\theta\, b\, dz \\ &= 2\,\rho g\, b\,\mathrm{Sin}\theta \sum_{z}(R - R_s)\,\Delta z \quad \ldots\ldots\ldots\ldots (11) \\ &= .39 \text{ lbs} \quad \text{(See Appendix 2)} \end{aligned}$$

From the calibration graph (Figure 10) the momentume measured for Q_j at 0.0081 ft^3/sec is approximately .383 lbs. Hence the error between the calculated and the measured readings is extremely small.

(C) A jet issuing through an exit, due to contraction and boundary effects, will neither maintain a uniform nor a parabolic velocity profile. For a uniform profile, the initial kinematic jet momentum per unit breadth is

$$J_u = A\,\frac{\overline{V}^2}{b},$$

A being the total jet area, $\overline{V}$ the uniform velocity, b the breadth. By substituting

$$\overline{V} = \frac{Q_j}{A}, \qquad b = \frac{10}{12} \text{ ft}, \quad \text{and} \quad A = .000475 \text{ ft}^2$$

one obtains,

$$J_u \doteq 2525.47\, Q_j^2 \quad \ldots\ldots\ldots\ldots\ldots\ldots (12)$$

For a parabolic profile, the initial kinematic jet momentum per unit breadth is

$$J_p = 1.333\, J_u = 3366.45\, Q_j^2 \quad \ldots\ldots\ldots\ldots (13)$$

since the momentum coefficient is 1.333 [11] .

One can then derive a chart as shown in Table 5 for the corresponding Q_j. By superimposing these results on the plot measured by the direct impinging method, one can obtain three curves as shown in Figure 14. These three curves are fitted, and the actual jet momentum is always higher than that of the uniform jet, which is to be expected.

(*D*) As described earlier, a few readings were taken with the jet discharging into air. Lower force readings were obtained for this case consistently as compared to the jet discharging into water due to surface tension effects (See Appendix 3). It was also observed that these effects had caused some flows discharging in air from individual tiny holes not to maintain parallel streams. The immersed jet as used in this study eliminates these undesirable effects.

Blockage Effect

In the Z-direction of the test section (Figure 8) the main stream is restricted by the top free surface and the bottom floor. The imposition of these boundaries caused the flow around a body placed in the test section to differ from that around the same body placed in an unlimited stream. For a counter jet, one may imagine a fictitous bluff body equivalent to the envelope created by the dividing streamline (Figure 2) in place of the jet. Thus, the influence of the boundary constraint due to the top and bottom limits will produce an increased X-direction velocity U' at the region of jet interaction. This implies that a higher flow velocity has to be attributed to the main stream than the value obtained by dividing the main flow rate by the cross section of the test section. The interference caused by the boundaries is generally denoted as blockage effect. This can affect the frequency data to a considerable extent.

To investigate the blockage effect, a series of measurements were carried out to cover a range of jet momentum J and main flow velocity U. The corresponding range of the specific Strouhal number and the specific Reynolds number were 0 to .5 and 1.2×10^3 to 1.5×10^5 respectively.

As explained earlier, the height H of the test section was always set at 5.417 ft, and the diameter d of the injection device was .0449 ft. Nevertheless, in conjunction with J and U^2, H provided a range of blockage number $\frac{J}{U^2H}$ up to .4.

Table 6 gives the corresponding velocities, frequencies, momentums measured and the equivalent values of S_s, R_s and B (See Appendix 2).

Figure 15 shows the overall plot of S_s versue B , and Figure 16 the overall plot of S_s versus R_s. Although there are a few scattered points, the general trend for the data to cluster around the curve drawn is clear.

In figure 15, the plot shows generally two regions, i.e. AB and BD, where B is about the transition point at which the curve starts levelling off.

In the region AB, the ratio of velocity $K = \overline{V}/\overline{U}$ is approximately under 20. It is apparent that the lower the K value, the higher the shedding frequency. In the limit, the vortex shedding frequency will be solely controlled by the size of the cylinder when jet flow is arrested. The region AB in Figure 15 where the jet momentum was low is dominated by the interference effects due to the presence of the injection device which happens to be the hollow cylinder.

From the experimental results reported[12] the body effect resulting from injection device of larger diameter presents a steeper slope in the region BC.

Figure 17 indicates that the non-dimensional distance w/d between the vortices increases as the ratio of velocity K increases. For a given d, H and U, this states that the wake gets blocked more and more as the jet velocity increases.

If one uses the characteristic length J/U^2 instead of the diameter d, and the parameter $B = \frac{J}{U^2 H}$ instead of K, one may draw a plot as the one shown in Figure 18. This relation indicates that for a given d and H, there is a value of B beyond which the blockage effect becomes evident. In the present case the point P as shown in Figure 18, is in the neighbourhood of

B = .04, which corresponds to the point B as shown in Figure 15.

It was declared that AB denoted interference region due to the injection device [12]. As such, BD denotes the blockage region. Clearly, up to a lower level of blockage, up to point C, the value of S_s increases slowly with B and in the region CD the blockage effect appears to be pronounced.

Tentatively one can state that the value of S_s for unblocked flows will be in the neighbourhood of 0.2 when body interference is absent (Asymptote ED).

A method of correcting the specific Strouhal number for blocked flow has been developed recently [13].

In Figure 15, points scattered in the region BD is apparent. Investigation determined that this condition was attributable to variations in measuring the main stream velocity U, where S_s and B are in inverse proportion to a 2 or 3 power of the value U. It was also attributable to the change-over of the jet manometer from carbon tetrachloride to mercury because the limited range of the former.

Wake Surveys and Vortex Shedding Frequency

Figures 20, 21 and 22 denote the wake survey charts corresponding to the preliminary tests [6] related to jet which had a 1/16" x 10" straight slot and was covered by a 7.75" cylindrical envelope over the jet in most of the instances. It is clear from Figure 20 that there was a distinct periodicity can be attributed to the counter jet oscillation [6]. The existence of jet oscillation was also present in the later test where a string of 1/32" diameter holes (Figure 4) constitute the counter jet. This is illustrated in Figure 23.

Figure 24 with variable Z indicates the intensity of turbulence decreases as one would expect at the region farther from the centre of the wake.

In the preliminary test with the straight slot jet (Figures 21 and 22) a modulation phenomenonwas observed. It is evident that for certain probe locations the signal of the jet oscillation predominates over the wake oscillations caused by vortex shedding of the solid body. Survey shown in Figure 22 indicates that the harmonics related to the cylinder vortex shedding is discernible. The arrows in Figure 22(d) indicate the vortex shedding frequency of the cylinder, which are detectable at certain locations of the lateral wake traverse.

Similar to Figure 18, if one uses the non-dimensional distance wU^2/J and the inverse of S_s instead of B, one may obtain a plot as shown in Figure 19. All points previously falling in the region BD where blockage effect is evident, are now clustered to a single line. It appears that for a given velocity U, the width w is inversely proportional to the shedding frequency n.

SUMMARY AND CONCLUSIONS

Results of this study may be summarized as follows:

(1) The instability of the plane counter jet leads to periodic jet oscillations.

(2) For a fixed stream velocity U, the scale of mixing increases with the jet momentum J. This fact is important in field applications.

(3) Blockage of flow in the jet wake comes to effect at point B (Figure 15) (corresponding to a value of $J/U^2H = .04$ in the present case) and becomes severe when J/U^2H reaches a value corresponding to point C.

(4) The asymptotic value of specific Strouhal number S_s is tentatively estimated to be in the neighbourhood of 0.2 when the jet is free from effects due to blockage and the size of the injection device.

(5) The direct measuring method of jet impact provides a very reliable procedure to estimate jet momentum.

(6) A string of holes may be used to replace slot on the jet injection device, since the former is easier to fabricate.

The test data lead us to conclude that $S_s = \frac{J\ n}{U^3}$ is constant when no body and blockage effects are present. This condition can be achieved by using a smaller injection device to prevent both these effects.

As such, for a given velocity of the main flow U, the frequency of wake oscillation of the jet, n, is inversely proportional to the jet momentum J. On the other hand, qualitatively the scale of turbulence is inversely proportional to the frequency of the velocity fluctation. This leads to the conclusion that increased jet momentum results in a higher scale of mixing.

SCOPE FOR FUTURE STUDIES

To determine the exact value of the specific Strouhal number which is expected to remain constant in a certain range of Block Number and specific Reynolds number, a better water tunnel capable of producing and maintaining a uniform main stream velocity and a higher rate of flow is recommended. Instruments for the velocity measurement should be conveniently arranged so that flow conditions can be monitored instantaneously when required.

A thorough survey is suggested of the main stream velocity across the test section to study the veloeity profile where blockage effect becomes evident. This information will provide a further understanding of the wake mixing characteristics.

The jet wake may be analyzed quantitatively to detect the dimensional relations of the vortex spacing and the size of mixing.

Future studies may include the test of plane counter jets of different jet fluids.

Digital methods may be employed to process data in a more efficient way (Figure 12).

TABLE 1 MAIN FLOW VELOCITY MEASUREMENT

ΔH (inch Hg)	n (cps)	U_{cal} (ft/sec)	U_{prop} (ft/sec)
2	1.85	.396	.395
4	2.48	.531	-
6	3.17	.678	-
8	3.60	.770	-
10	4.00	.856	-
12	4.33	.927	.929

ΔH = total difference in height of mercury column in the manometer

n = vertex shedding frequency behind the .539" cylindrical injection device

U_{cal} = the local main flow velocity calculated from Strouhal number, $U_{cal} = .2139n$, $d = .0449$ ft

U_{prop} = the local main flow velocity measured by using the mini-flowmeter.

TABLE 2 CALIBRATION OF JET METERING ORIFICE

Δh (inch ccl_4)	wt (lb)	T (sec)	$Q_j = \frac{wt}{T}$ (ft^3/sec)	$\overline{V} = \frac{Q_j}{A}$ (ft/sec)
3.8	15	102.2	.00235	5.52
7.4	20	95.25	.00335	7.71
14.0	30	106.0	.00453	10.62
19.8	40	118.6	.00540	12.65
26.3	40	102.75	.00624	14.65
32.0	40	92.85	.00690	16.20
40.8	40	81.5	.00786	18.45
47.2	40	75.75	.00846	19.90

Δh = total difference in height of ccl_4 in the manometer

wt = weight of water discharged and collected

T = time taken to collect a set weight of water discharged

Q_j = rate of the jet flow through the orifice

$\overline{V}$ = mean jet velocity

A = total area of jet holes, $\pi(\frac{0.033}{2 \times 12})^2$ 80 or .000426 ft^2

TABLE 3 RECORD OF JET MOMENTUM MEASUREMENT

Δh (inch ccl_4)	Q_J (ft^3/sec)	wt (gram)	F (lb)	J (ft^3/sec^2)
6.0	.00300	45.4	.0500	.0310
8.0	.00347	61.3	.0676	.0418
10.0	.00386	77.1	.0850	.0526
12.0	.00420	91.1	.1004	.0621
14.0	.00452	103.6	.1142	.0706
16.0	.00484	121.7	.1341	.0830
18.0	.00515	135.9	.1498	.0927
22.0	.00571	165.8	.1828	.1131
26.0	.00621	195.3	.2153	.1332
30.1	.00669	225.0	.2480	.1535
34.2	.00715	257.0	.2833	.1753
40.2	.00775	299.1	.3297	.2040
48.2	.00851	355.3	.3916	.2423
	.01415	2.06 lbs.	1.03 lbs.	.6300

Δh = total difference in height of ccl_4 in the manometer

wt = weight to counter balance the jet momentum

F = actual force on the jet impinging plate, wt/2, in lbs.

J = kinematic jet momentum per unit breadth, $F/\rho b$, b being the total breadth of the jet, 10 inches.

TABLE 4 JET VELOCITY PROFILE MEASUREMENT IN TERMS OF WATER HEAD

Z (cm)	ΔZ (cm)	R (cm)	$R - R_s$ (cm)	$(R - R_s)\Delta Z$ (cm^2)
1.9		14.8	0.0	
	.6			.03
1.3		14.7	0.1	
	.1			.03
1.2		14.5	0.3	
	.1			.05
1.1		14.3	0.5	
	.1			.11
1.0		13.7	1.1	
	.1			.21
.9		12.7	2.1	
	.1			.33
.8		11.5	3.3	
	.1			.48
.7		10.0	4.8	
	.1			.63
.6		8.5	6.3	
	.1			.82
.5		6.6	8.2	
	.1			.99
.4		4.9	9.9	
	.1			1.21
.3		2.7	12.1	
	.1			1.30
.2		1.8	13.0	
	.1			1.35
.1		1.3	13.5	
	.1			1.38
0.0		1.0	13.8	
	.1			1.38
-.1		1.0	13.8	
	.1			1.33
-.2		1.5	13.3	
	.1			1.20
-.3		2.4	12.0	
	.1			1.11
-.4		3.7	11.1	
	.1			.93
-.5		5.5	9.3	
	.1			.80
-.6		6.8	8.0	
	.1			.67

(to be continued)

TABLE 4 (CONTINUED)

Z (cm)	ΔZ (cm)	R (cm)	$R - R_s$ (cm)	$(R - R_s)\Delta Z$ (cm^2)
-.7		8.1	6.7	
	.1			.52
-.8		9.6	5.2	
	.1			.39
-.9		10.9	3.9	
	.1			.28
-1.0		12.0	2.8	
	.1			.17
-1.1		13.1	1.7	
	.1			.11
-1.2		13.7	1.1	
	.1			.05
-1.3		14.3	0.5	
	.1			.03
-1.4		14.5	0.3	
	.1			.01
-1.5		14.7	0.1	
	.1			.005
-1.6		14.75	0.05	
	.1			.00
-1.7		14.8	0.0	

$\Sigma (R - R_s)\Delta Z = 17.905$

Z = vertical location of the total head tube; set Z = 0 at the centre line of the injection device.

ΔZ = difference between two adjacent Z settings

R = actual reading on the capillary tube, in cm.

R_s = actual reading of the static pressure, 14.8 cm.

Note: Scales on the capillary tube were in reverse order.

TABLE 5 J_u AND J_p

Q_j (ft^3/sec)	J_u (ft^3/sec^2)	J_p (ft^3/sec^2)
.002	.01010	.01465
.003	.02272	.03029
.004	.04040	.05386
.005	.06313	.08416
.006	.09091	.12119
.007	.12374	.16495
.008	.16163	.21545

Q_j = rate of the jet flow

J_u = initial kinematic jet momentum per unit breadth with uniform velocity profile

J_p = initial kinematic jet momentum per unit breadth with parabolic velocity profile

Example:

$Q_j = .005 \ ft^3/sec$

$J_u = 2525.47 \ Q_j^2 = 2525.47 \times .000025 = .06313 \ ft^3/sec^2$

$J_p = 1.333 \ J_u = 3366.45 \ Q_j^2 = 3366.45 \times .000025$

$= .08416 \ ft^3/sec^2$

TABLE 6 U , J , n , S_s , B , AND R_s

H, height = 5.417 ft
d, diameter = .0449 ft

U (ft/sec)	J (ft^3/sec^2)	n (sec^{-1})	$S_s = \frac{J\,n}{U^3}$	$B = \frac{J}{U^2 H}$	$R_s = \frac{J}{\nu U}$ (x 10^3)
.927	.0101	4.0	.0507	.0022	1.00
	.0203	2.57	.0655	.0044	2.03
	.0304	2.25	.0859	.0065	3.01
	.0517	2.08	.1347	.0111	5.12
	.0720	1.78	.1604	.0155	7.12
	.1024	1.32	.1697	.0220	10.14
	.1445	1.08	.1963	.0310	14.32
	.1826	0.875	.2006	.0392	18.08
	.2084	0.795	.2080	.0448	20.69
	.6389	0.316	.2534	.1373	63.25
	.8519	0.244	.2609	.1830	84.40
	1.0649	0.213	.2841	.2288	105.50
	1.1714	0.198	.2912	.2516	116.10
.92	.2130	0.729	.1994	.0465	21.30
	.4260	0.422	.2309	.0929	42.70
	.6389	0.316	.2593	.1393	64.00
	.8519	0.259	.2834	.1858	85.30

(to be continued)

TABLE 6 (Continued)

H, height = 5.417 ft
d, diameter = .0449 ft

U (ft/sec)	J (ft^3/sec^2)	n (sec^{-1})	$S_s = \frac{J\,n}{U^3}$	$B = \frac{J}{U^2 H}$	$R_s = \frac{J}{\nu\,U}$ (x 10^3)
.856	.0112	3.5	.0625	.0028	1.20
	.0213	2.25	.0764	.0054	2.28
	.0309	2.0	.0985	.0078	3.31
	.0507	1.91	.1544	.0128	5.43
	.0710	1.39	.1575	.0179	7.60
	.1014	1.11	.1794	.0255	10.85
	.1435	0.84	.1915	.0362	15.36
	.1826	0.696	.2026	.0460	19.55
	.5325	0.320	.2717	.1342	57.00
	.7454	0.232	.2757	.1878	79.98
	1.0649	0.184	.3124	.2683	114.10
	1.1714	0.167	.3119	.2951	125.40
.770	.0112	3.2	.0785	.0035	1.33
	.0157	2.14	.0736	.0049	1.87
	.0208	1.82	.0829	.0065	2.48
	.0304	1.69	.1125	.0095	3.62
	.0517	1.43	.1622	.0161	6.16
	.0700	1.065	.1633	.0218	8.34
	.1014	0.80	.1777	.0316	12.10
	.1420	0.688	.2138	.0442	16.92

(to be continued)

TABLE 6 (Continued)

H, height = 5.417 ft
d, diameter = .0449 ft

U (ft/sec)	J (ft^3/sec^2)	n (sec^{-1})	$S_s = \frac{J\,n}{U^3}$	$B = \frac{J}{U^2 H}$	$R_s = \frac{J}{\nu\,U}$ (x 10^3)
.770	.1826	0.552	.2208	.0569	21.75
	.2231	0.454	.2219	.0695	24.39
	.6389	0.205	.2869	.1989	76.10
	.8519	0.162	.3123	.2652	101.50
	1.0649	0.149	.3476	.3316	127.00
.678	.1065	0.496	.1695	.0428	14.40
	.2130	0.298	.2037	.0855	28.80
	.4259	0.1875	.2562	.1710	57.60
	.6389	0.1428	.2927	.2566	86.50
	.8519	0.1259	.3441	.3421	115.55
.531	.0101	1.2	.0810	.0066	1.74
	.0203	1.09	.1478	.0133	3.51
	.0507	0.592	.2005	.0332	8.76
	.0912	0.331	.2018	.0598	15.78
	.1597	0.20	.2133	.1046	27.60
	.2130	0.178	.2532	.1395	36.80
	.3195	0.126	.2689	.2092	55.20
	.6389	0.096	.4114	.4183	110.40
	.8519	0.092	.5235	.5578	147.10

TABLE 7 SIZE OF SHEDDING IN THE WAKE

ΔH (in Hg)	U (ft/sec)	Δh in ccl_4	J (ft^3/sec^2)	$K = \overline{V}/\overline{U}$	$W = w/d$	U^3/Jn	$B = \frac{J}{U^2 H}$	wU^2/J
12	.927	2.0	.0101	3.4	5.6	19.70	.0021	21.9
		10.2	.0517	10.5	12.1	7.42	.0111	8.9
		20.2	.1024	15.2	16.7	5.89	.0217	6.5
		28.5	.1445	17.9	24.1	5.10	.0310	6.2
		41.0	.2079	21.6	29.7	4.80	.0446	5.5
		126.0	.6388	38.0	59.4	3.95	.1372	3.5
		168.0	.8518	43.2	74.2	3.84	.1829	3.3
		210.0	1.0647	49.1	89.1	3.52	.2287	3.2
10	.856	2.2	.0111	5.3	9.3	16.00	.0028	27.6
		10.0	.0507	11.1	14.8	6.48	.0127	9.7
		28.3	.1435	19.7	22.3	5.22	.0361	5.1
		36.0	.1825	21.4	27.8	5.94	.0459	5.0
		105.0	.5324	37.2	63.1	3.68	.1341	3.9
		147.0	.7453	43.7	81.6	3.53	.1877	3.6
		210.0	1.0647	52.5	100.2	3.20	.2682	3.1
		231.0	1.1712	55.0	111.3	3.20	.2950	3.1
8	.770	2.2	.0111	5.7	7.4	12.74	.0034	17.9
		13.8	.0699	14.3	20.4	6.12	.0217	7.8
		20.0	.1014	17.5	25.9	5.62	.0300	7.2
		28.0	.1419	21.0	30.0	4.68	.0441	5.6
		36.0	.1825	23.2	33.4	4.52	.0568	4.8
		44.0	.2231	25.8	37.1	4.51	.0694	4.4
		126.0	.6388	44.1	64.9	3.49	.1988	2.7
6	.4596	21.0	.1065	19.6	37.1	5.90	.0427	7.7
		42.0	.2129	27.6	55.7	4.91	.0855	5.4
		84.0	.4259	40.7	70.5	3.90	.1710	3.4
		126.0	.6388	49.0	81.6	3.42	.2565	2.6
		168.0	.8518	55.9	89.1	2.90	.3421	2.2
4	.2819	4.0	.0202	9.6	14.8	6.76	.0132	9.3
		10.0	.0517	15.5	26.0	4.98	.0338	6.3
		18.0	.0903	27.0	37.1	4.15	.1395	3.6
		44.0	.2231	33.0	55.7	3.95	.1461	3.1
		63.0	.3194	38.2	70.5	3.72	.2091	2.7

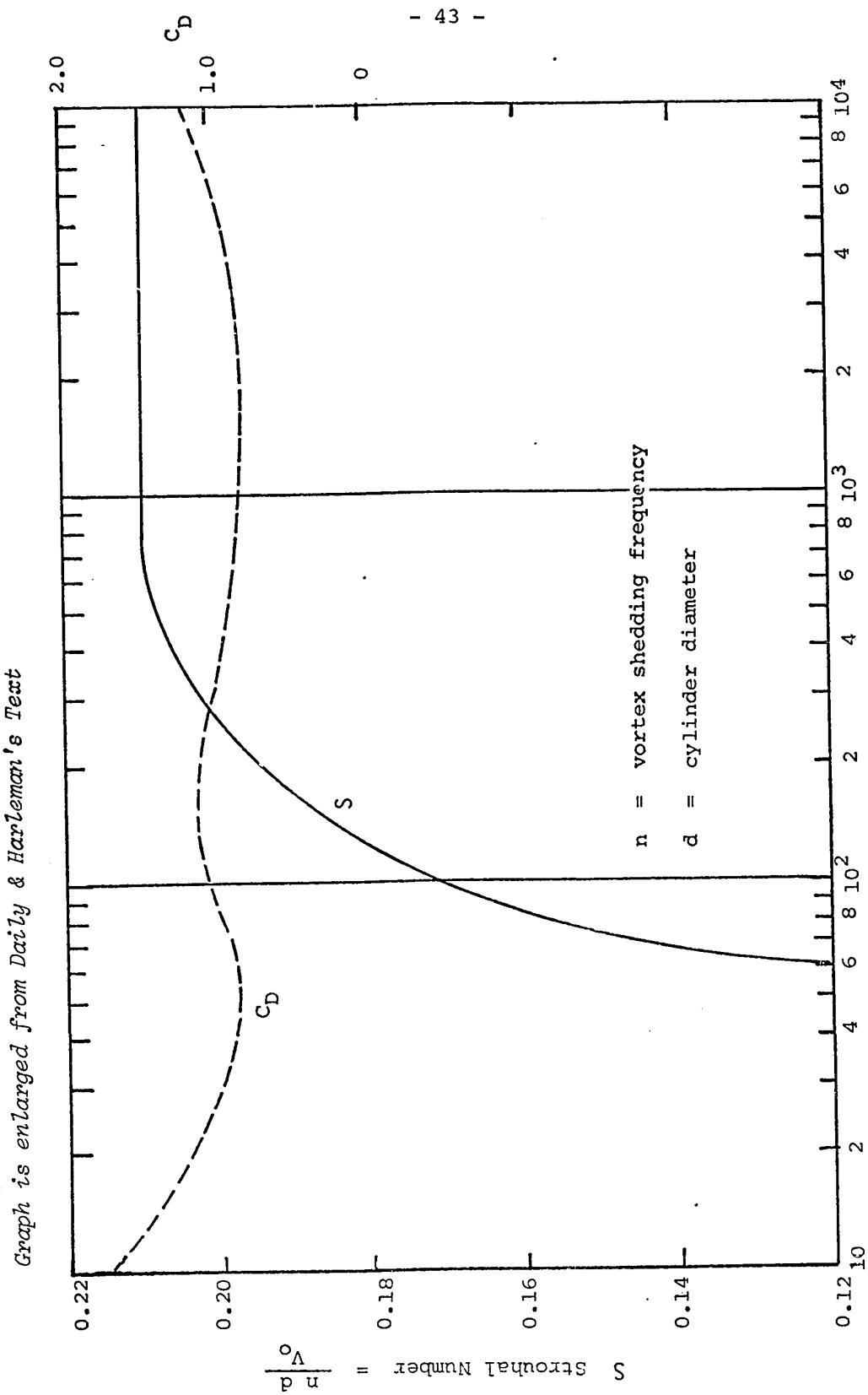

FIGURE 1 STROUHAL NUMBER AND DRAG COEFFICIENT VERSUS REYNOLDS NUMBER FOR CIRCULAR CYLINDERS

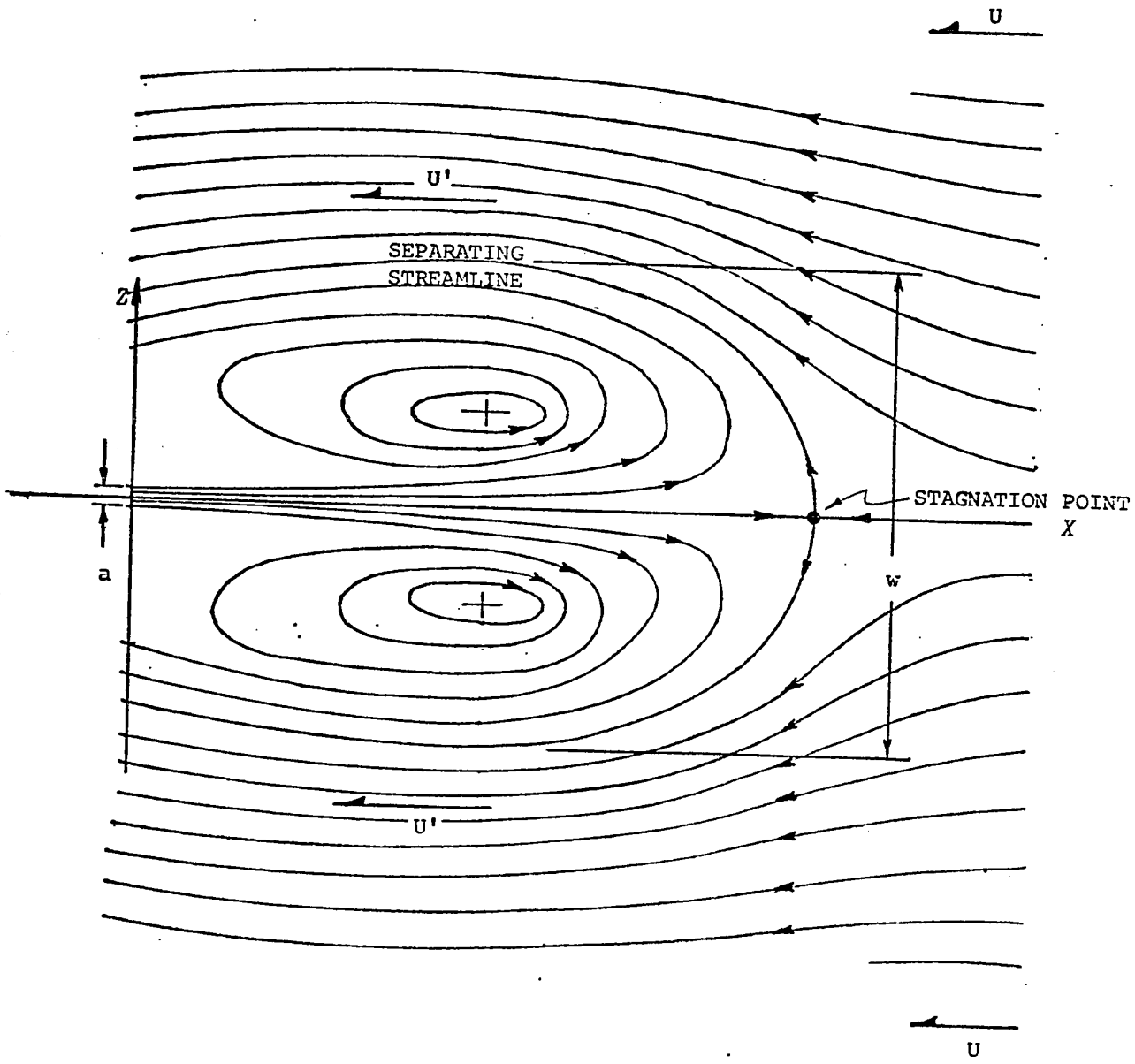

FIGURE 2 FLOW PATTERN OF A COUNTERJET - TRANSFORMED FROM COLIN'S PAPER OF WALL JET IN A COUNTER FLOW

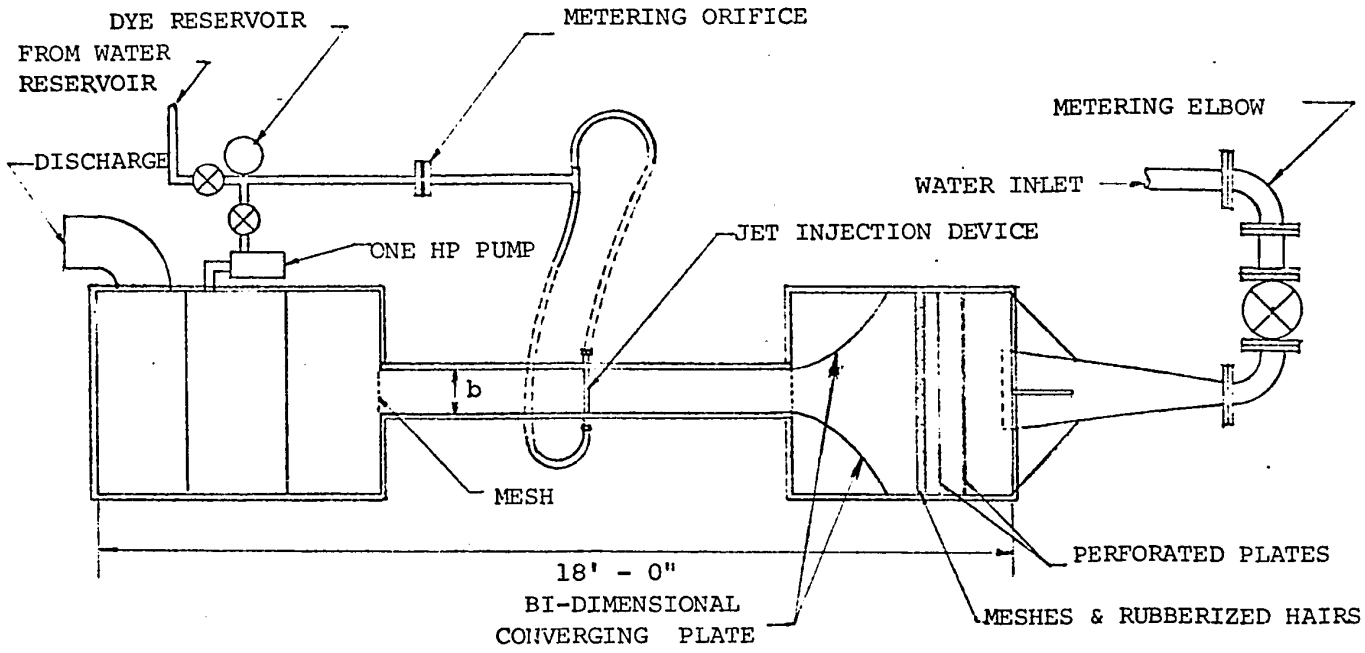

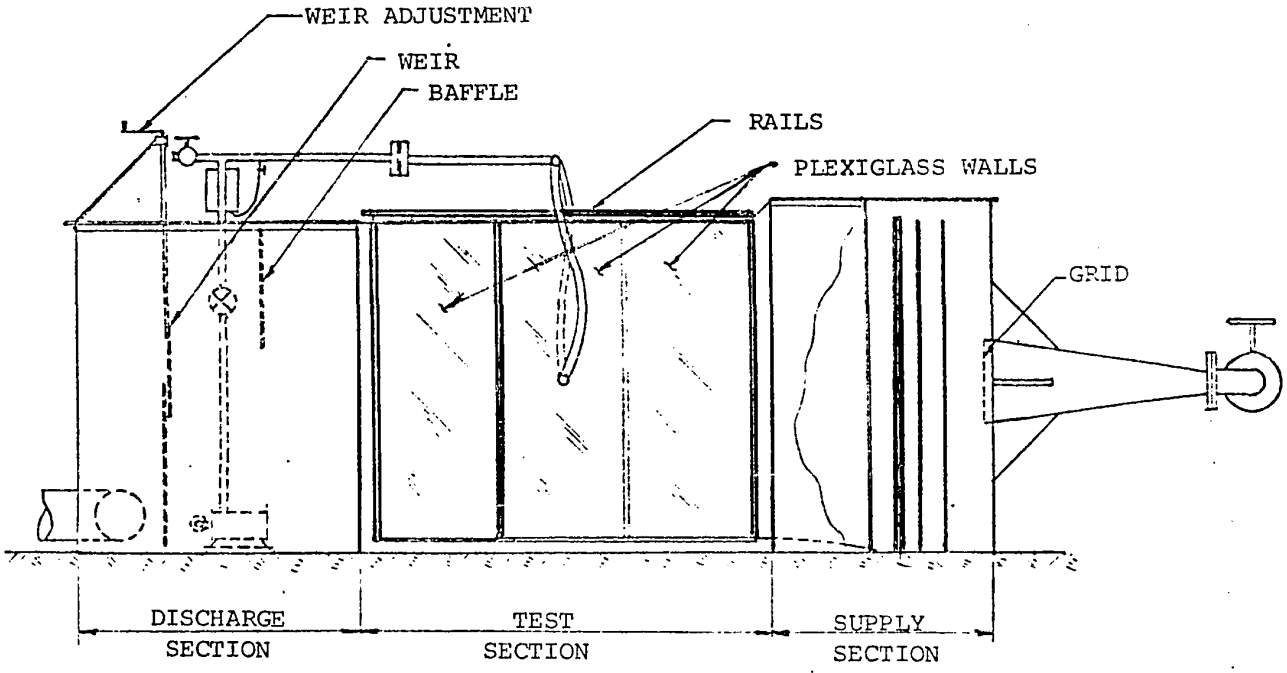

FIGURE 3 WATER TUNNEL

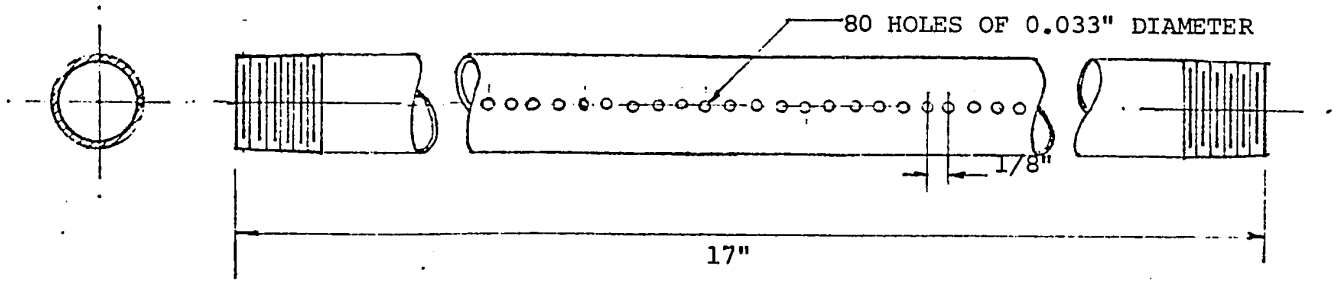

JET INJECTION TUBE

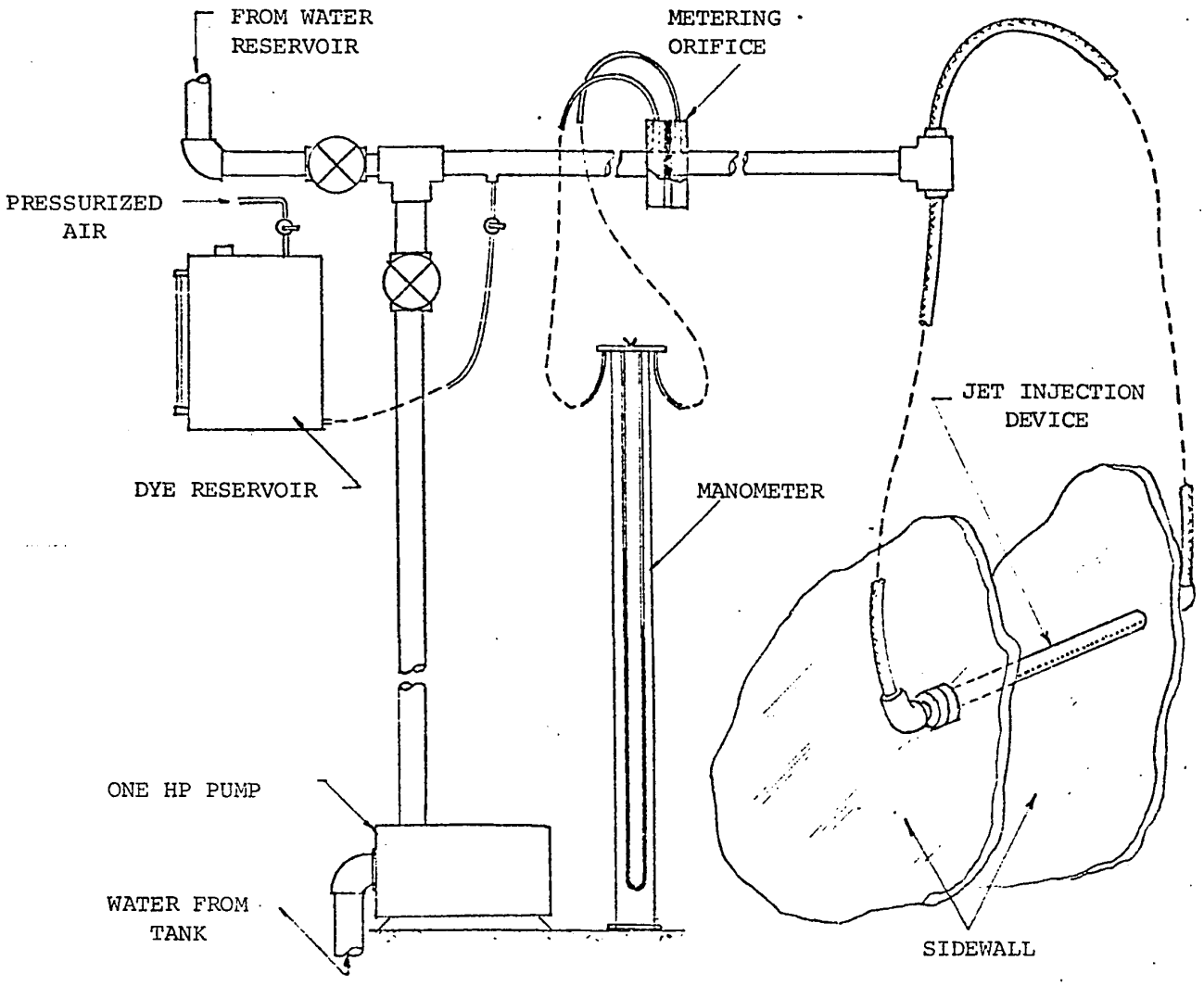

FIGURE 4 INJECTION SYSTEM

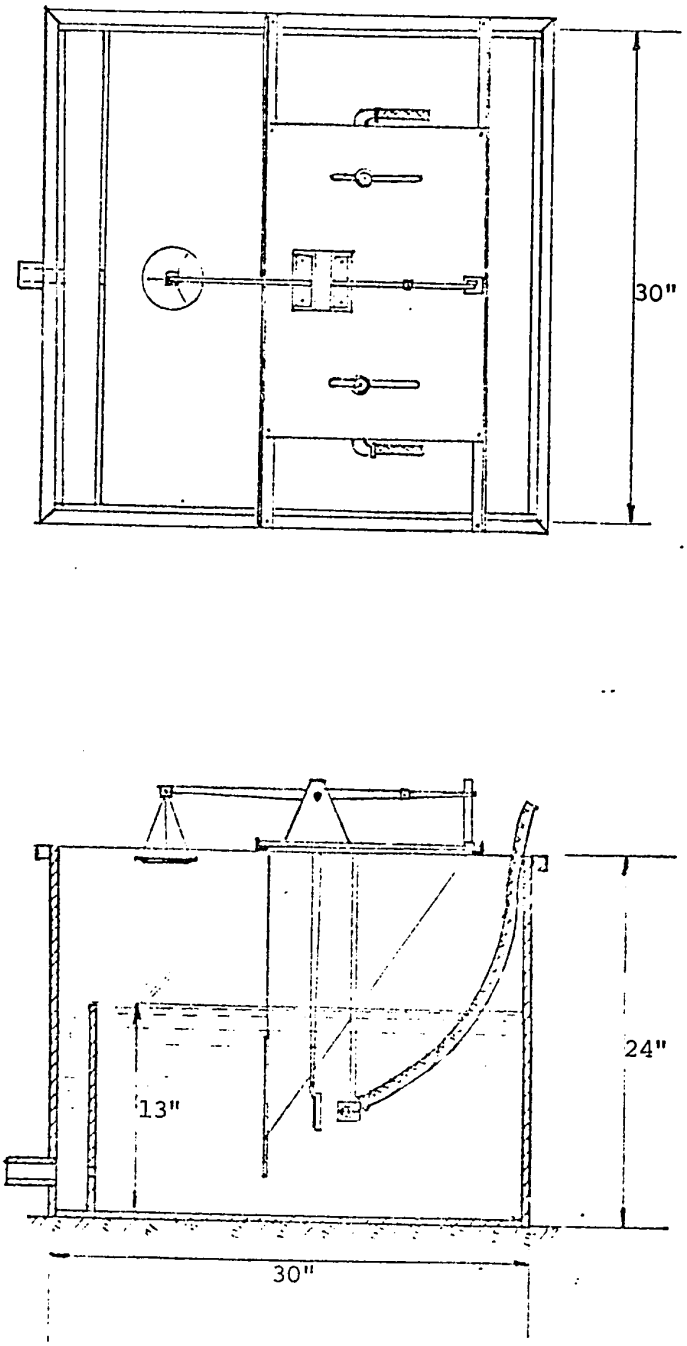

FIGURE 5 MOMENTUM CALIBRATION SET-UP

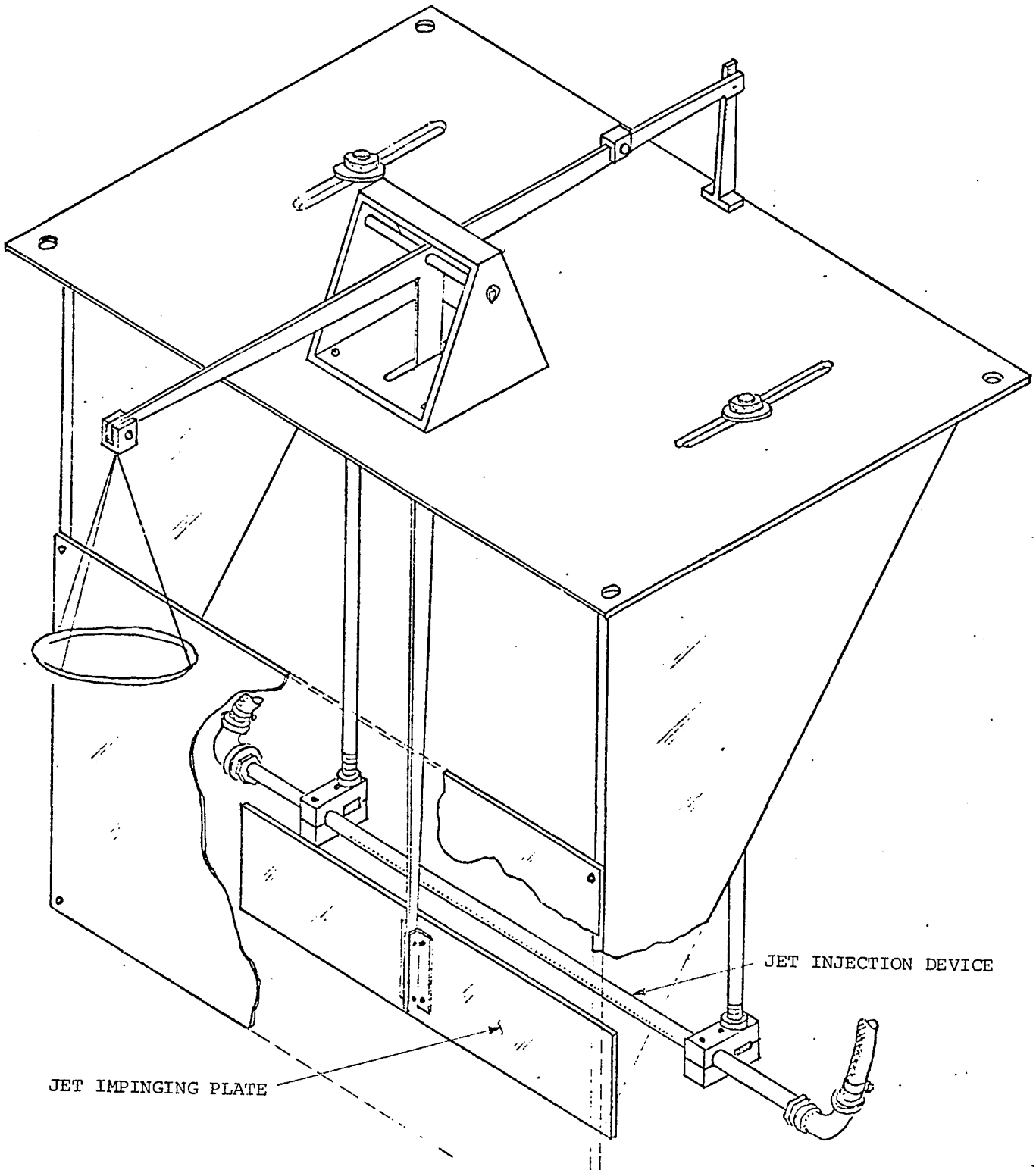
JET INJECTION DEVICE
JET IMPINGING PLATE
BALANCE ASSEMBLY

FIGURE 6

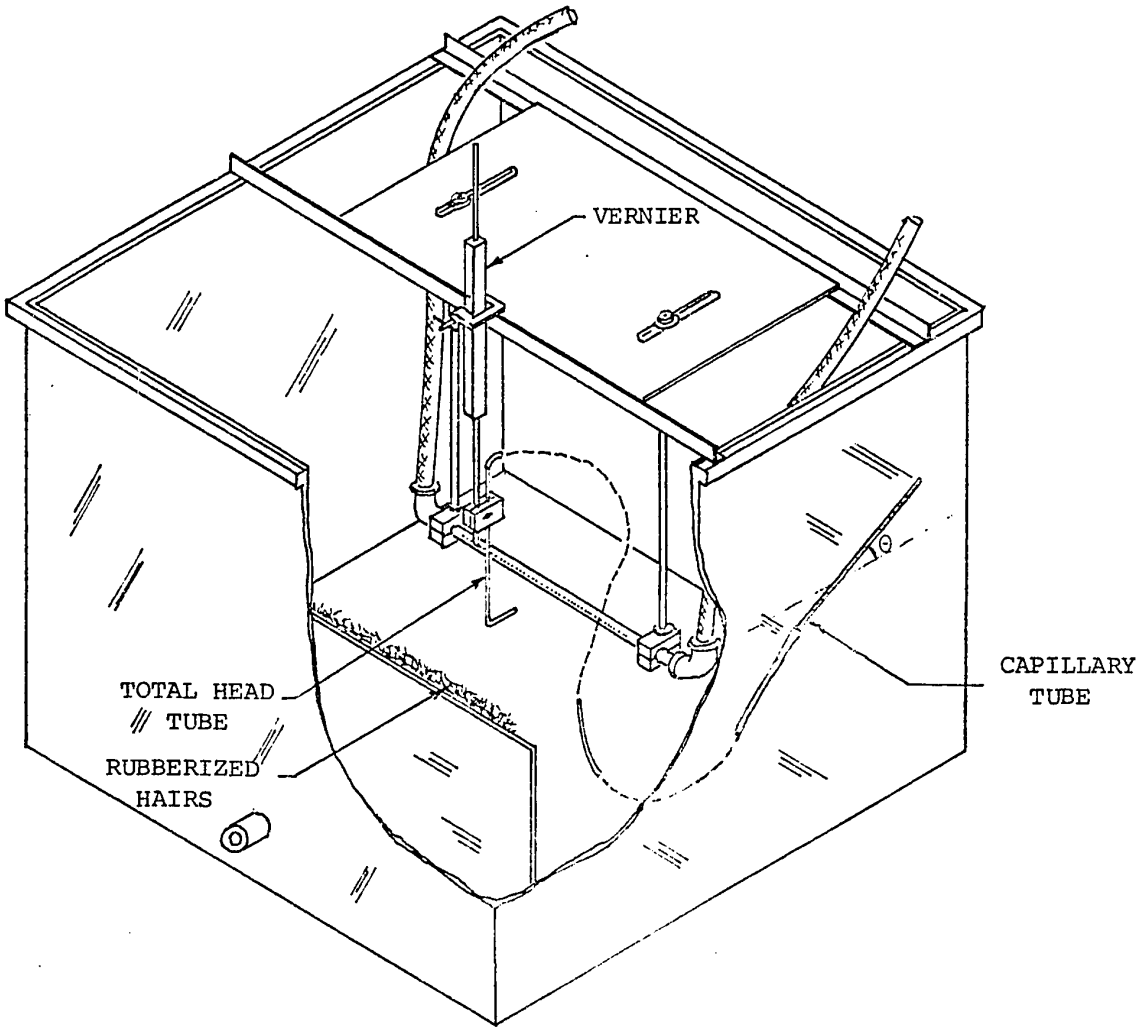

FIGURE 7 TOTAL HEAD TUBE INSTALLATION

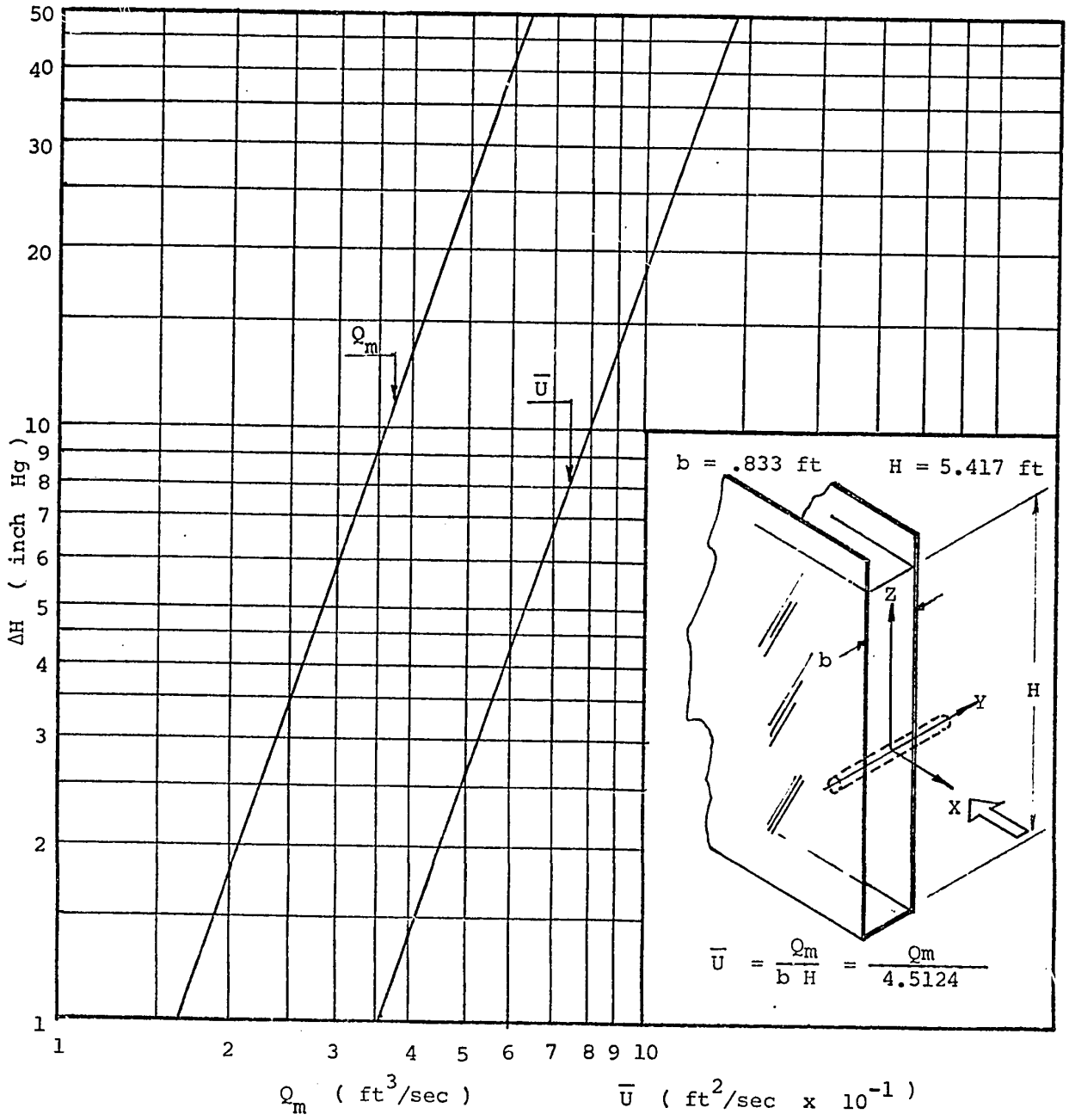

FIGURE 8 Q_m AND $\overline{U}$ VERSUS ΔH

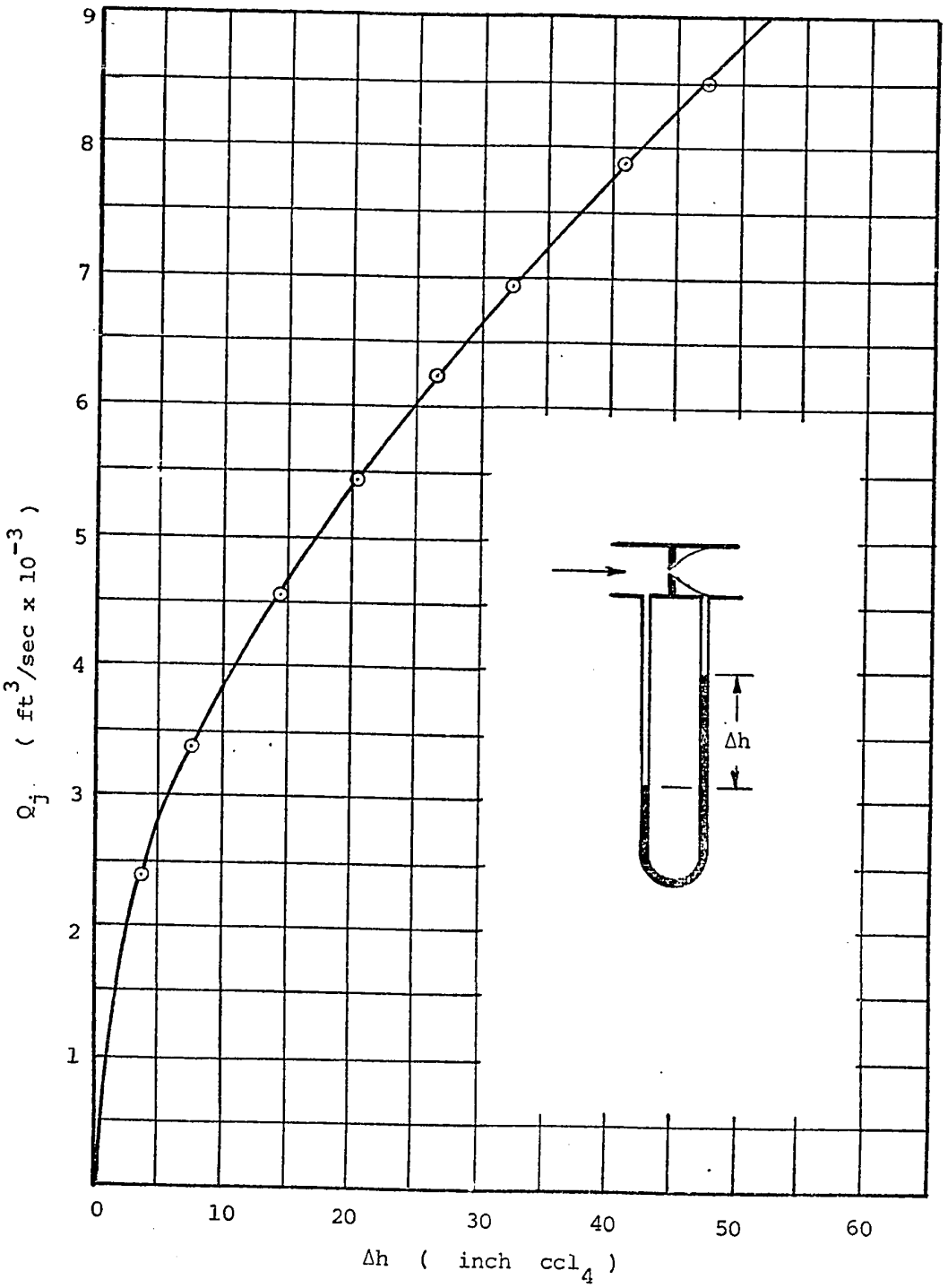

FIGURE 9 Δh VERSUS Q_J

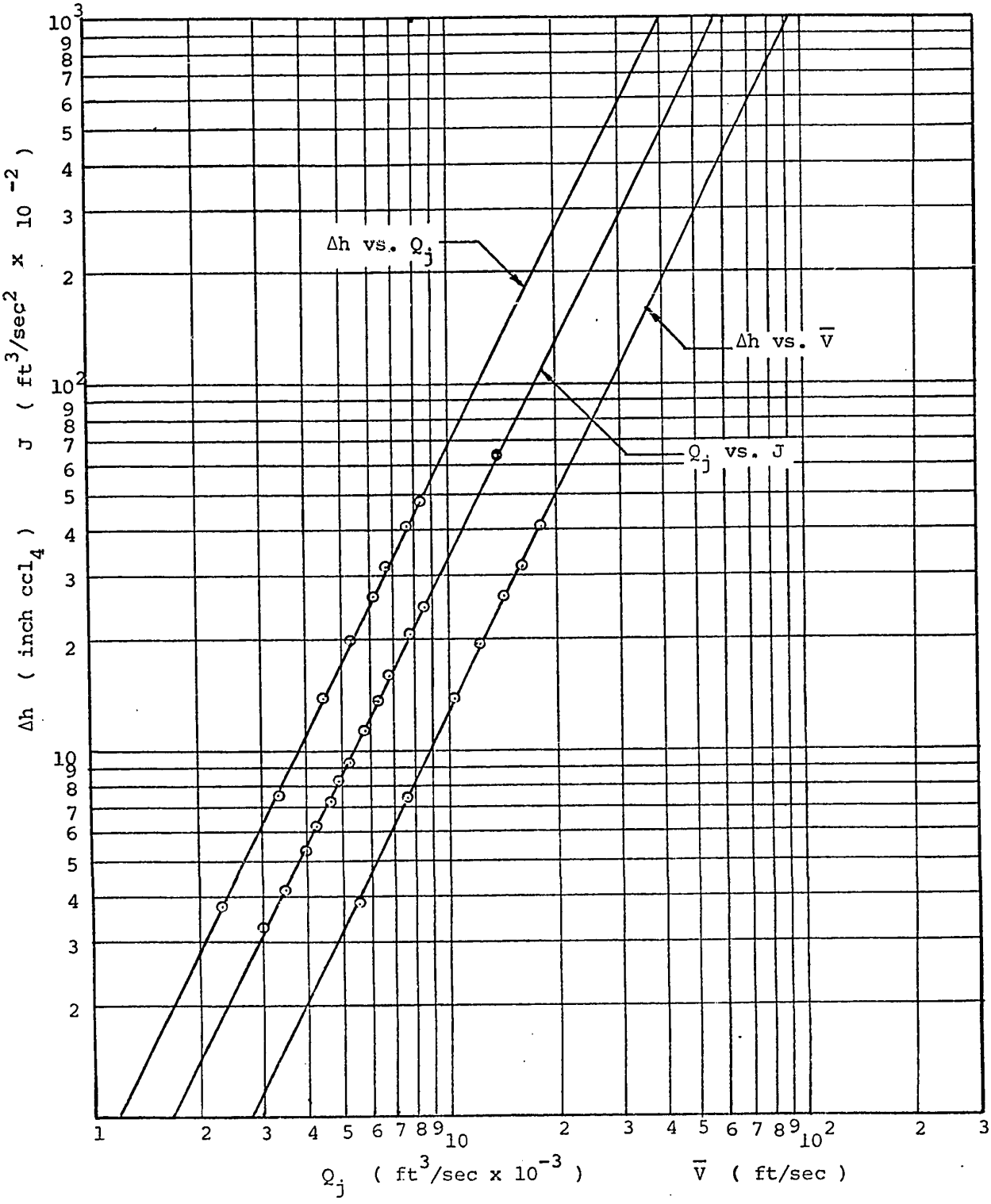

FIGURE 10 Q_j AND $\bar{V}$ VERSUS Δh, AND Q_j VERSUS J

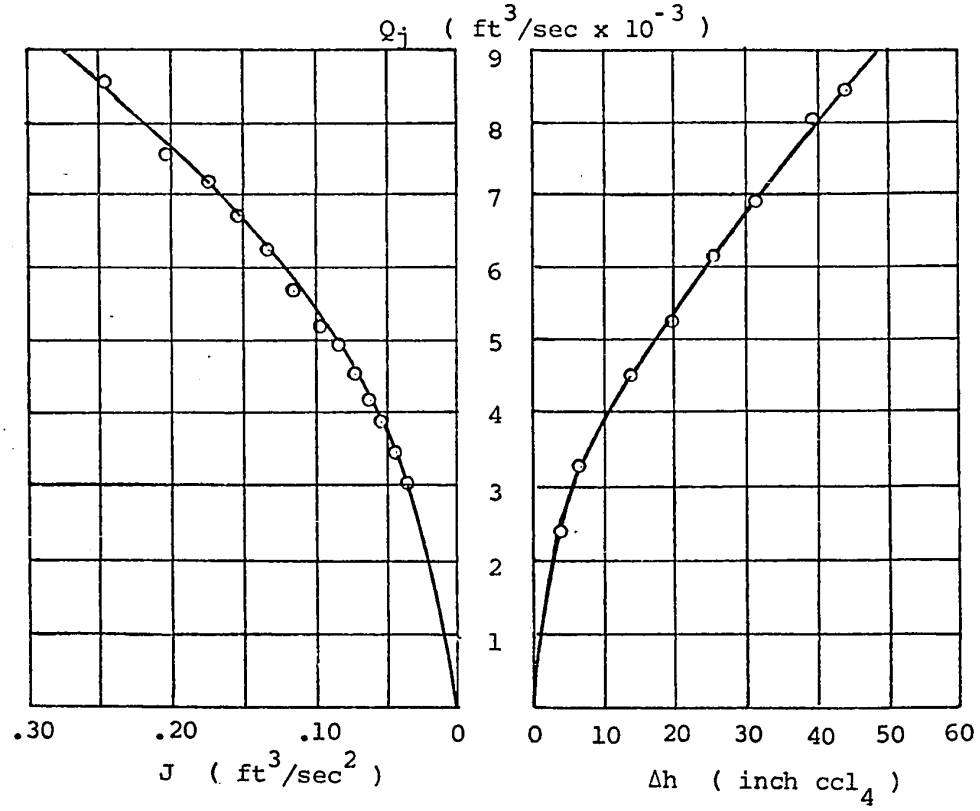

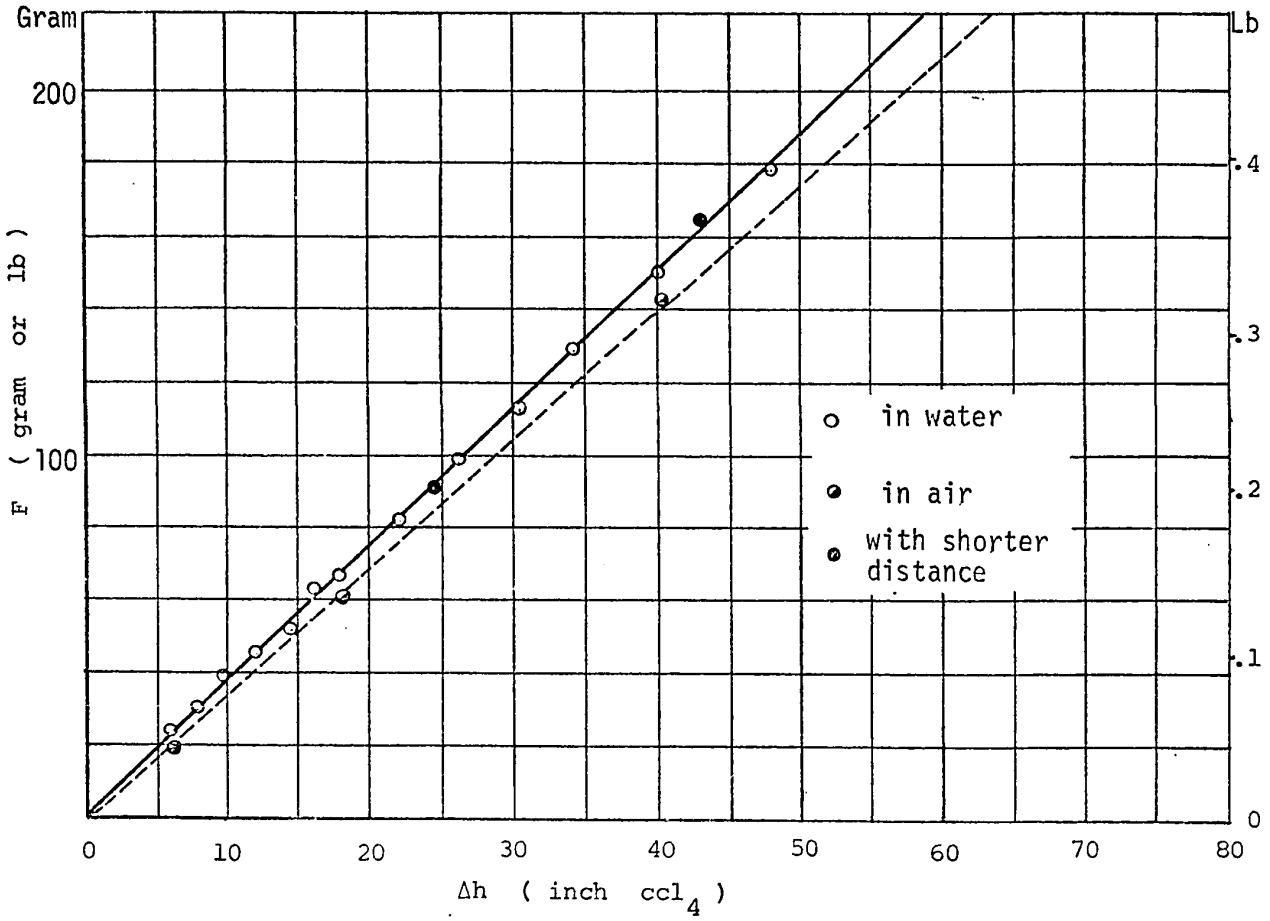

FIGURE 11 JET MOMENTUM

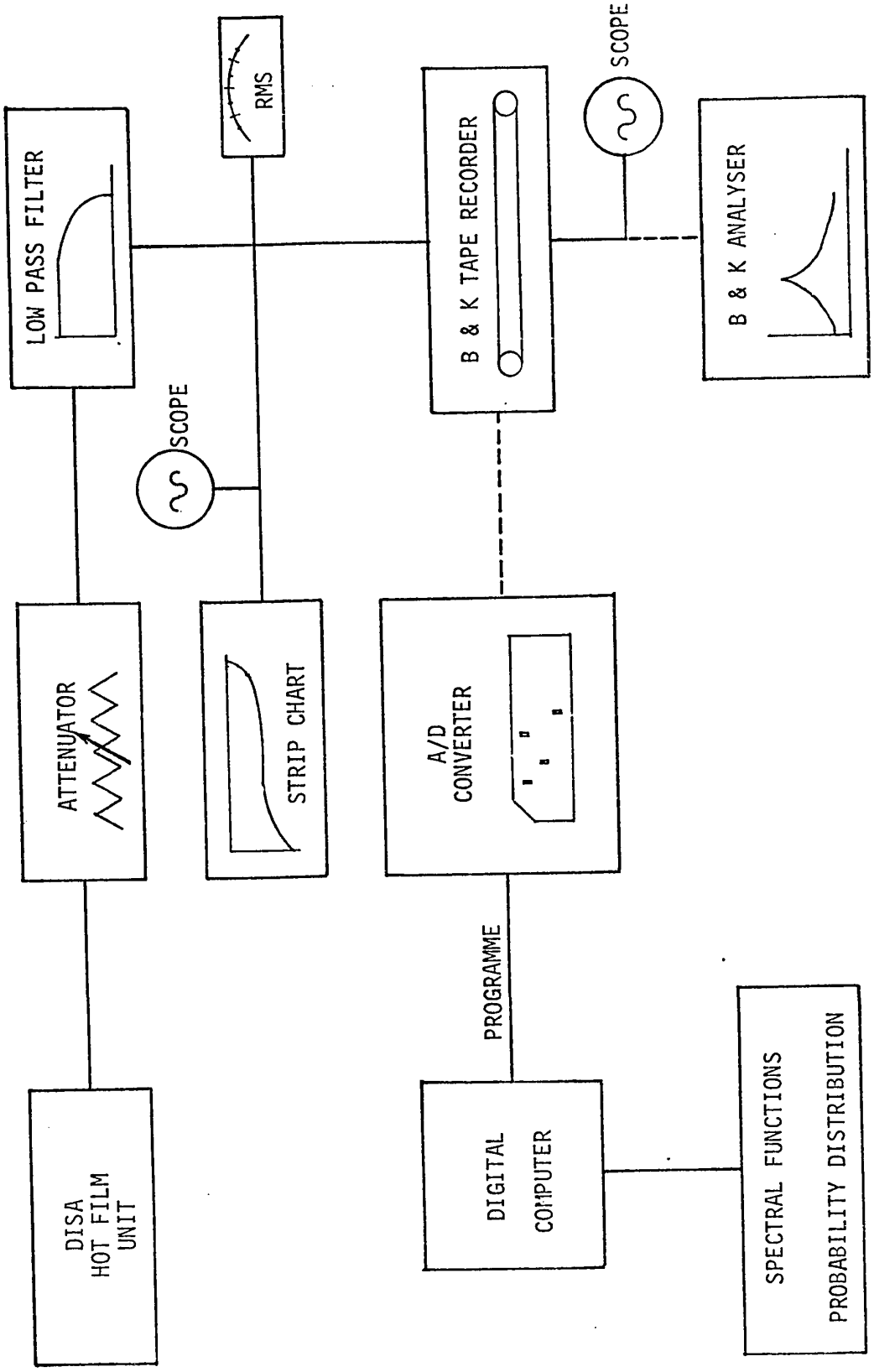

FIGURE 12 ELECTRONIC INSTRUMENTATION

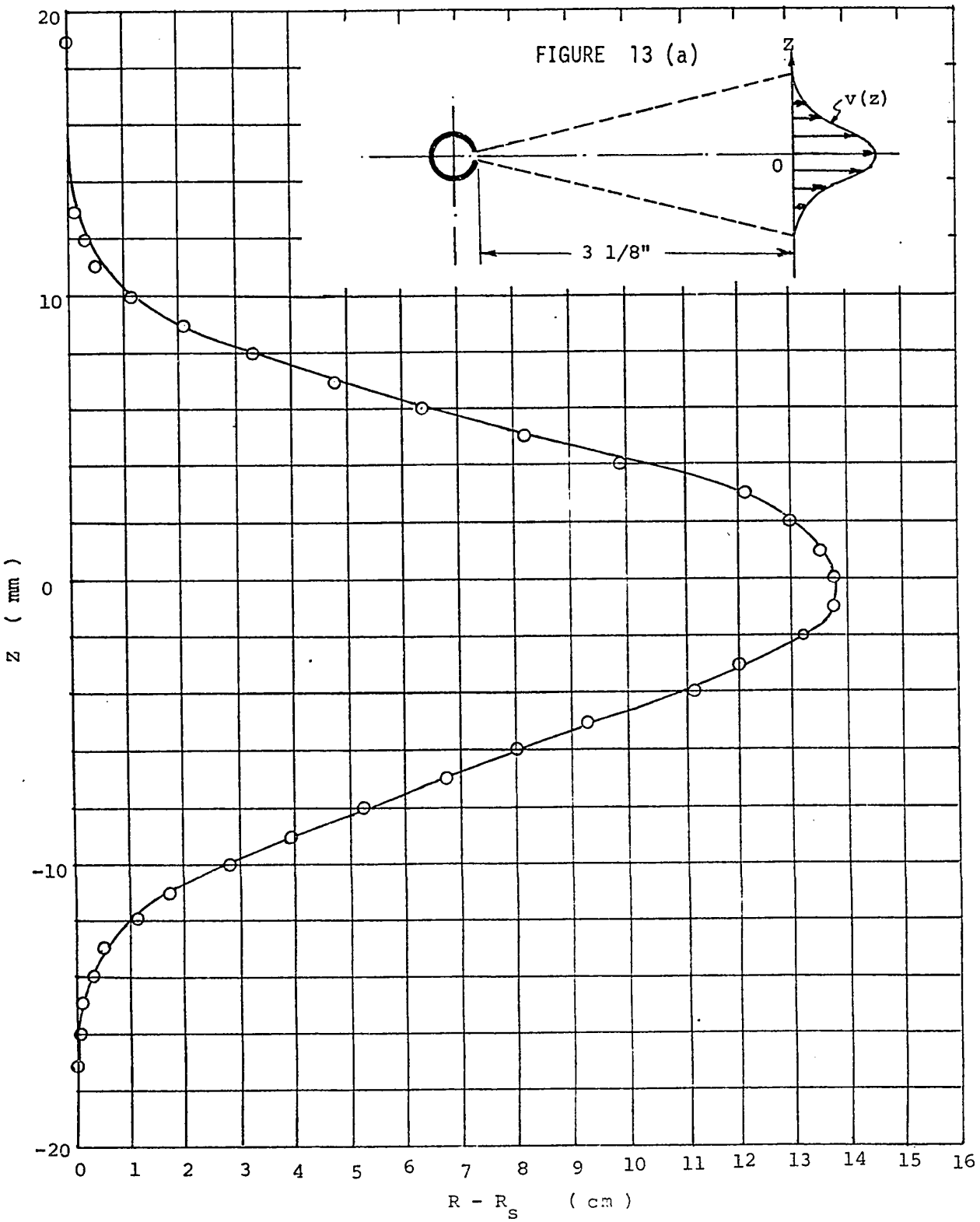

FIGURE 13 JET VELOCITY PROFILE

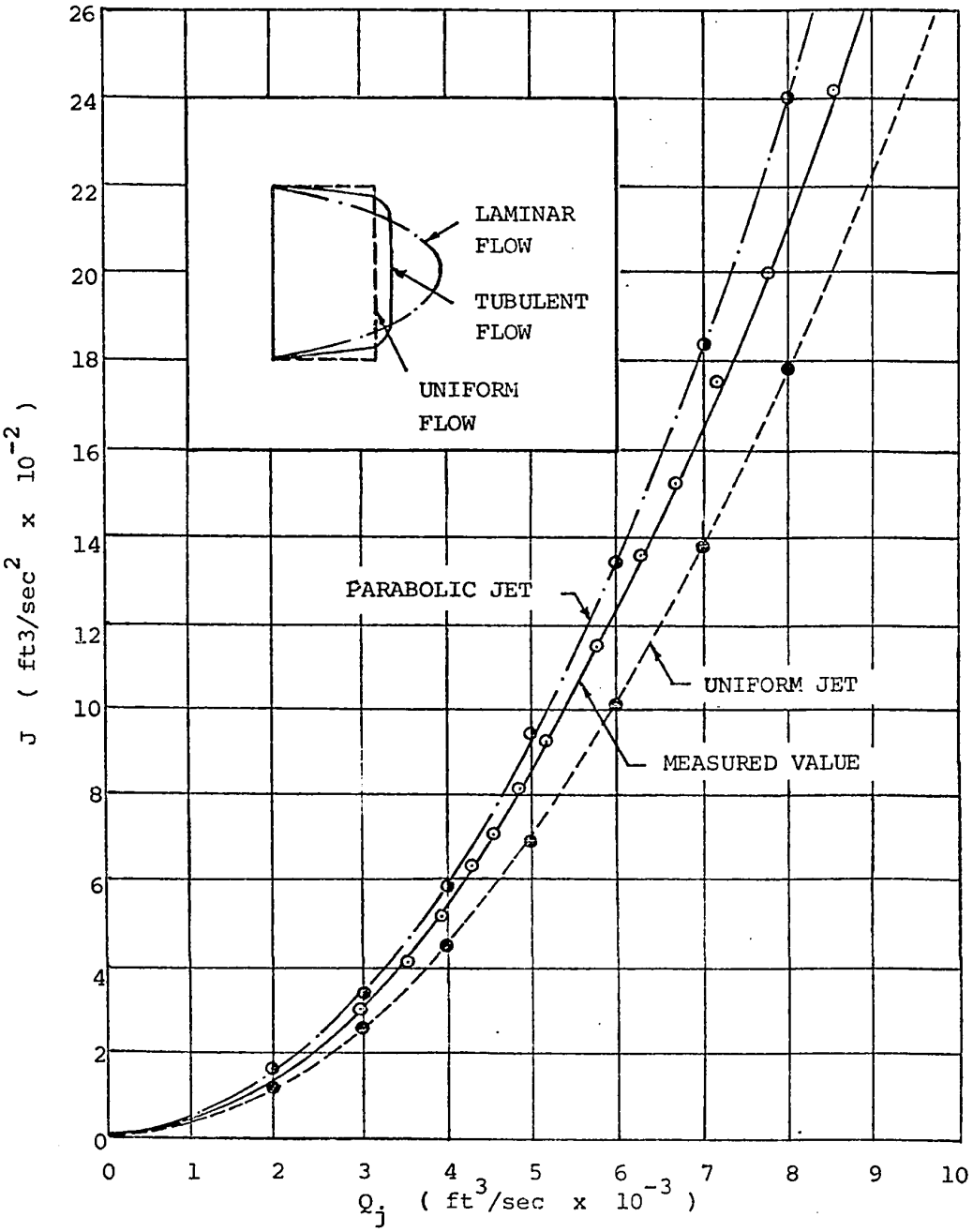

FIGURE 14 Q_j VERSUS J

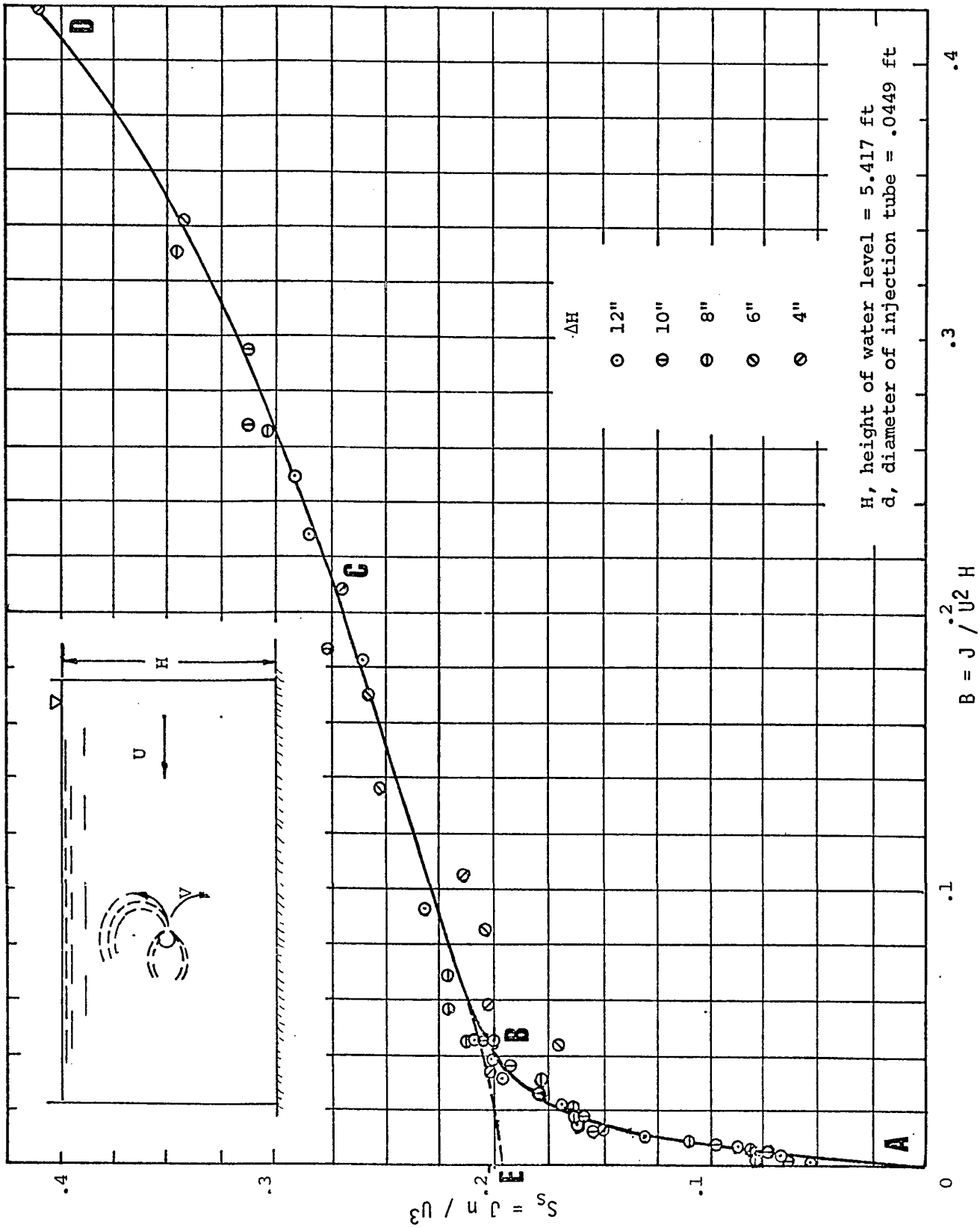

FIGURE 15 S_s VERSUS B

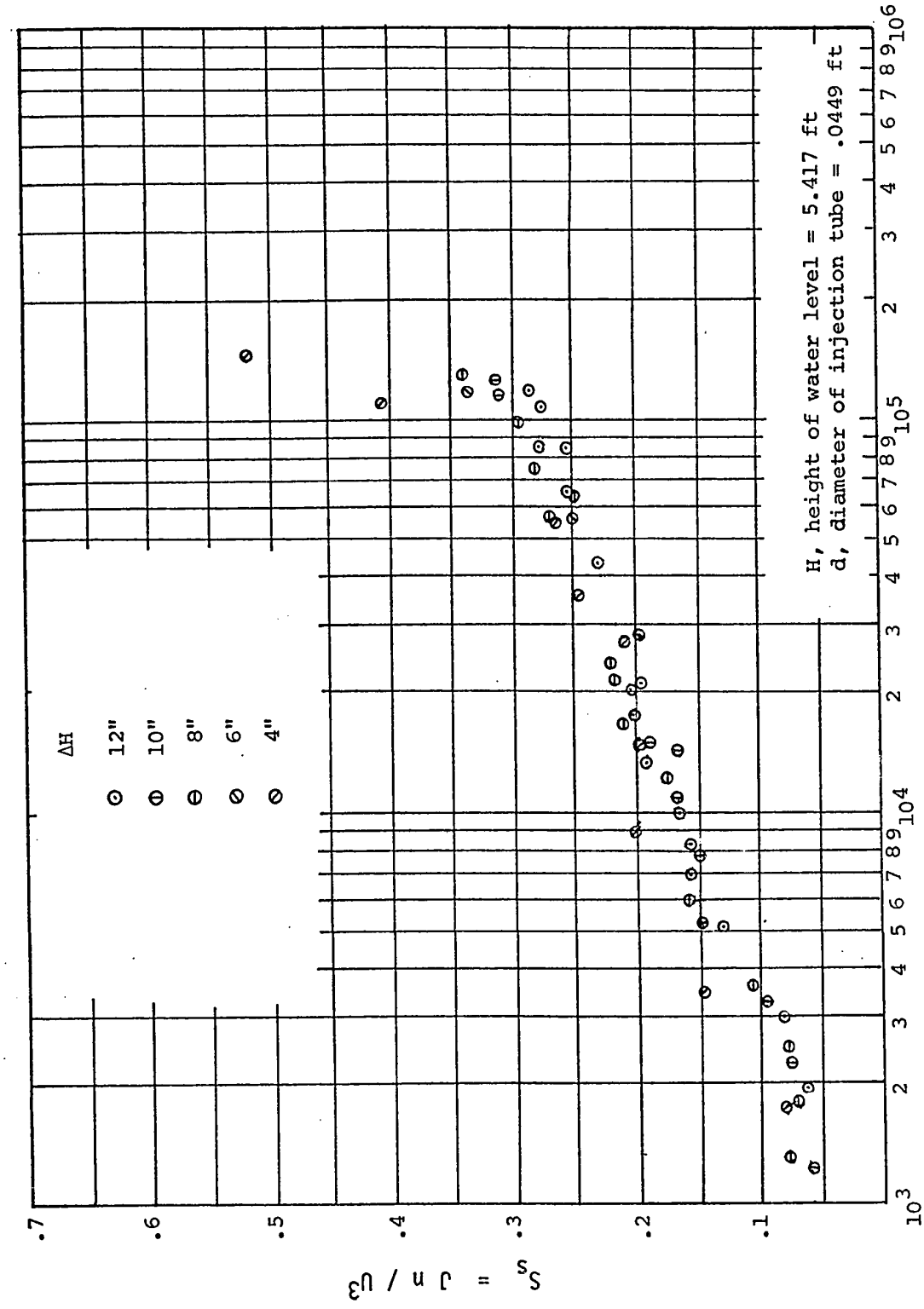

FIGURE 16 S_s VERSUS R_s

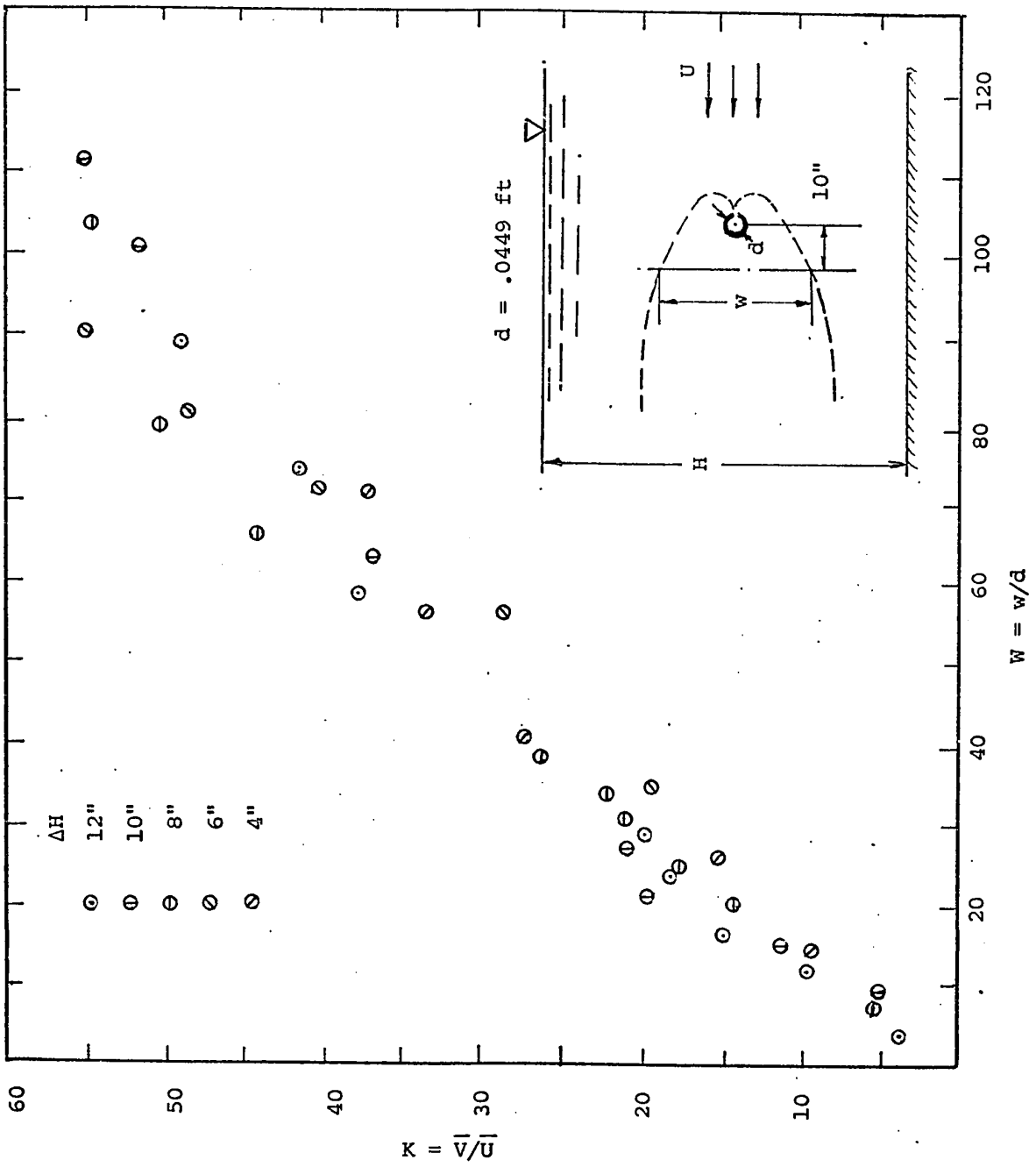

FIGURE 17 SIZE OF SHEDDING IN THE WAKE

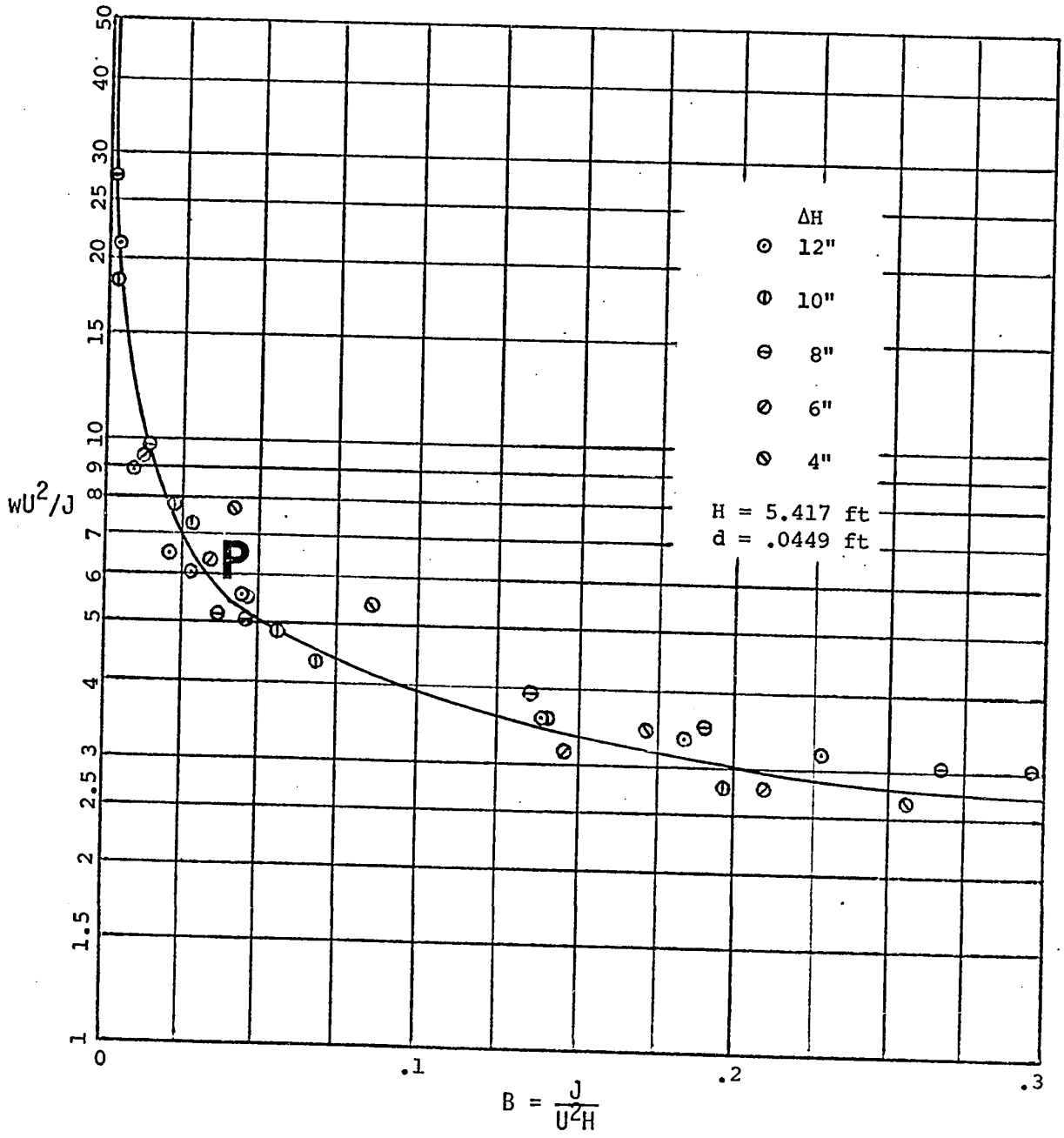

FIGURE 18 B VERSUS wU^2/J

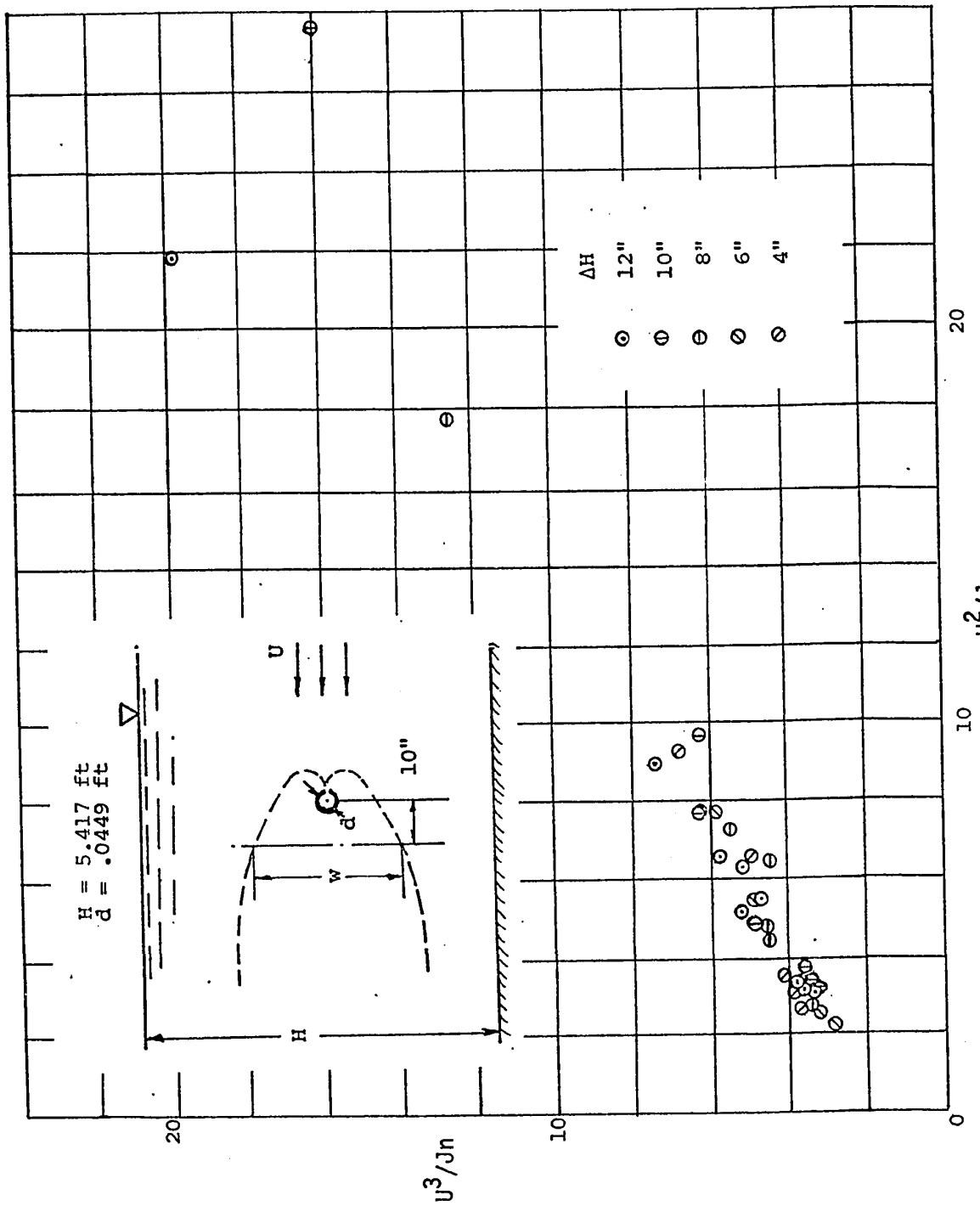

FIGURE 19 U^3/Jn VERSUS wU^2/J

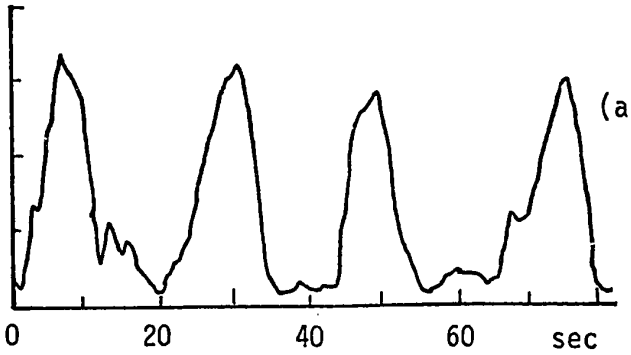

(a) V = 12.3 ft/sec n = 0.0475 cycle/sec
U = 0.463 ft/sec

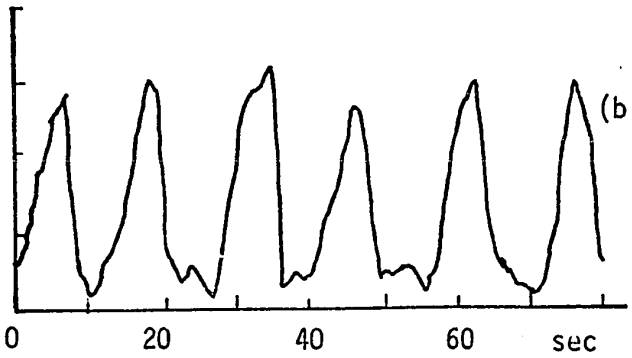

(b) V = 12.3 ft/sec n = 0.0720 cycle/sec
U = 0.57 ft/sec

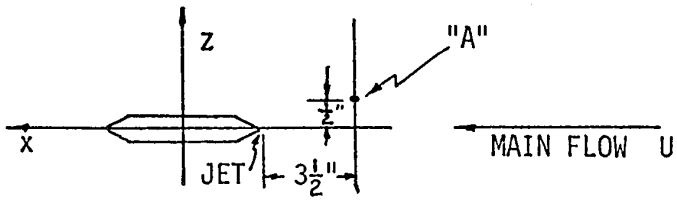

FIGURE 20 HOT FILM RECORD AT POINT "A" - JET ONLY

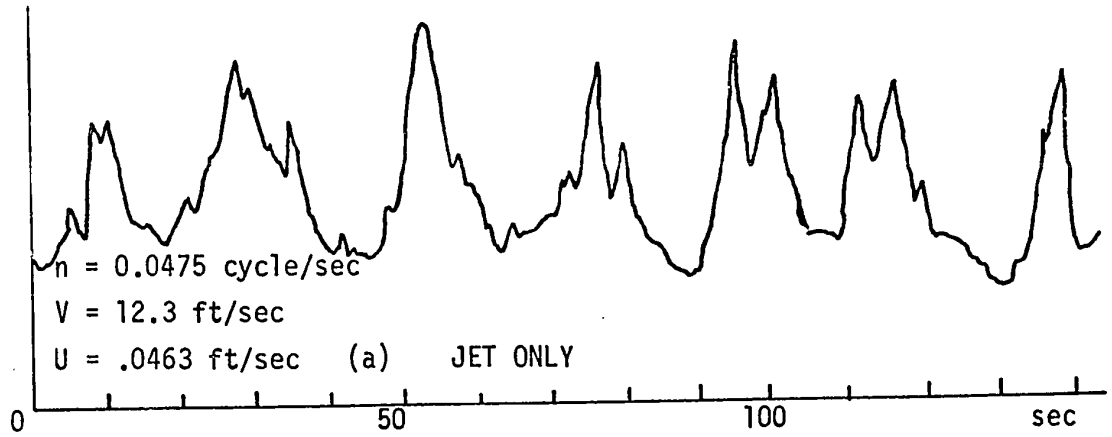

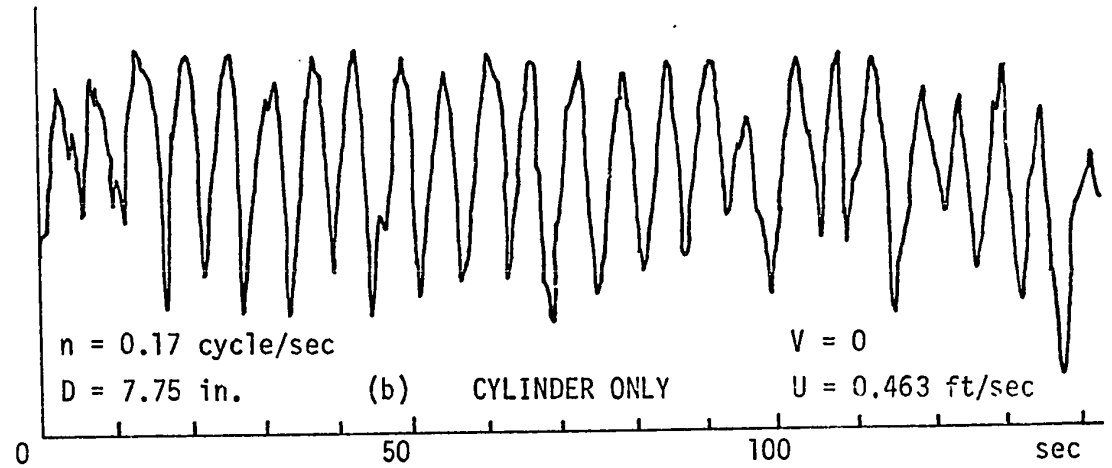

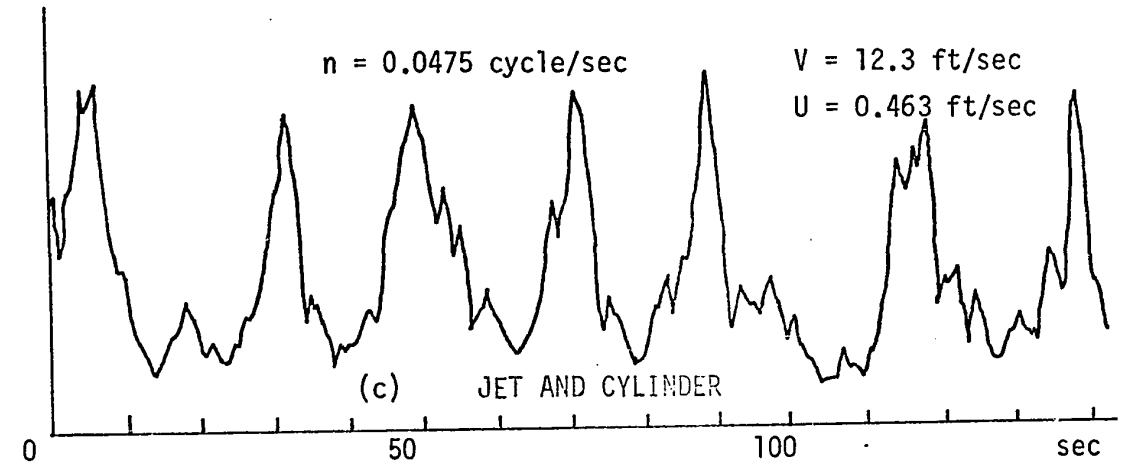

D = 7.75 in.

$\frac{X}{D}$ = 1.74

$\frac{Z}{D}$ = 0.28

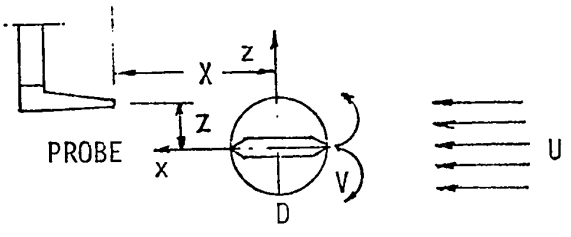

FIGURE 21 HOT FILM SURVEYS - JET ONLY, CYLINDER ONLY, AND JET AND CYLINDER

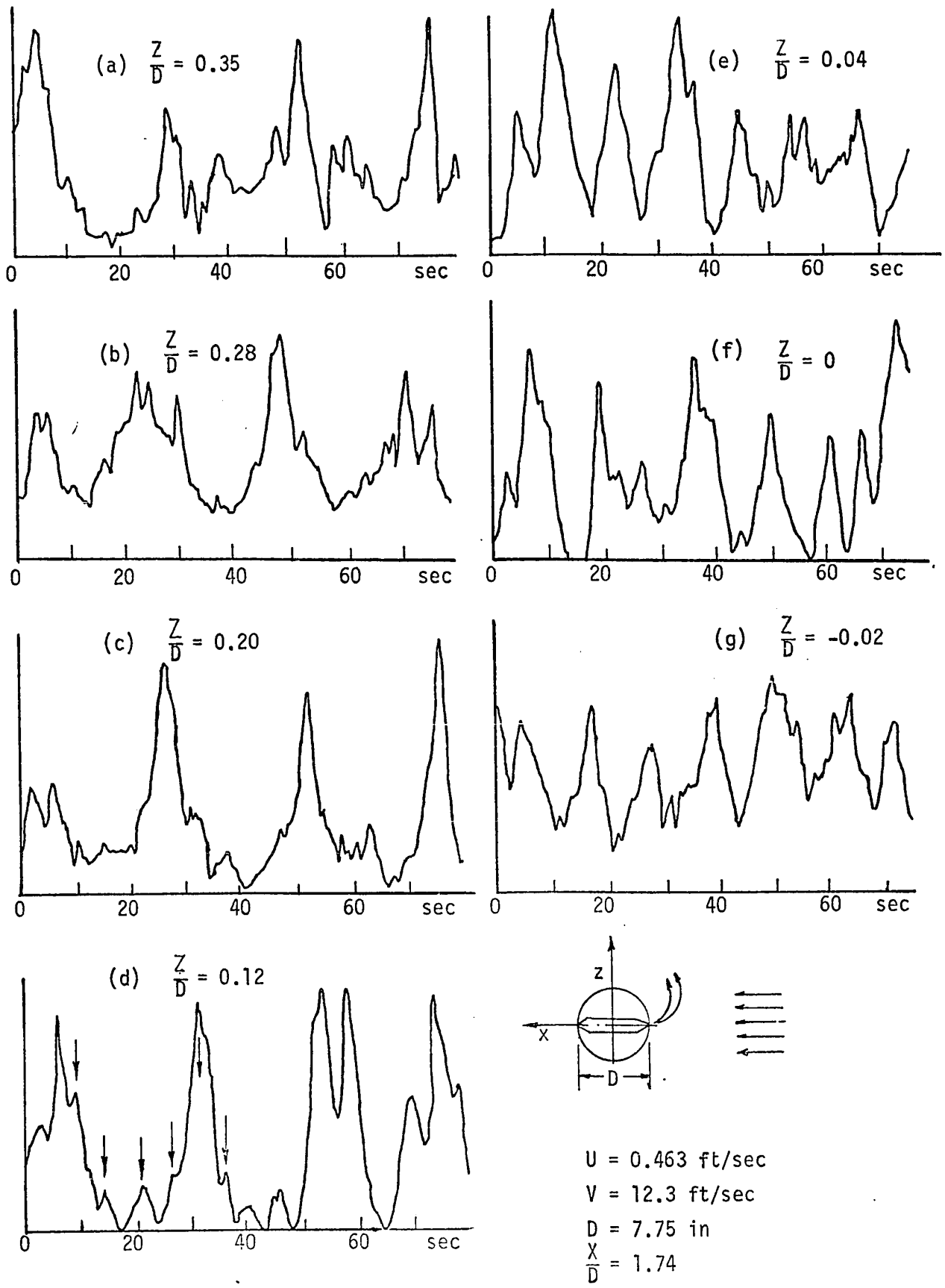

FIGURE 22 HOT FILM SURVEYS - JET AND CYLINDER

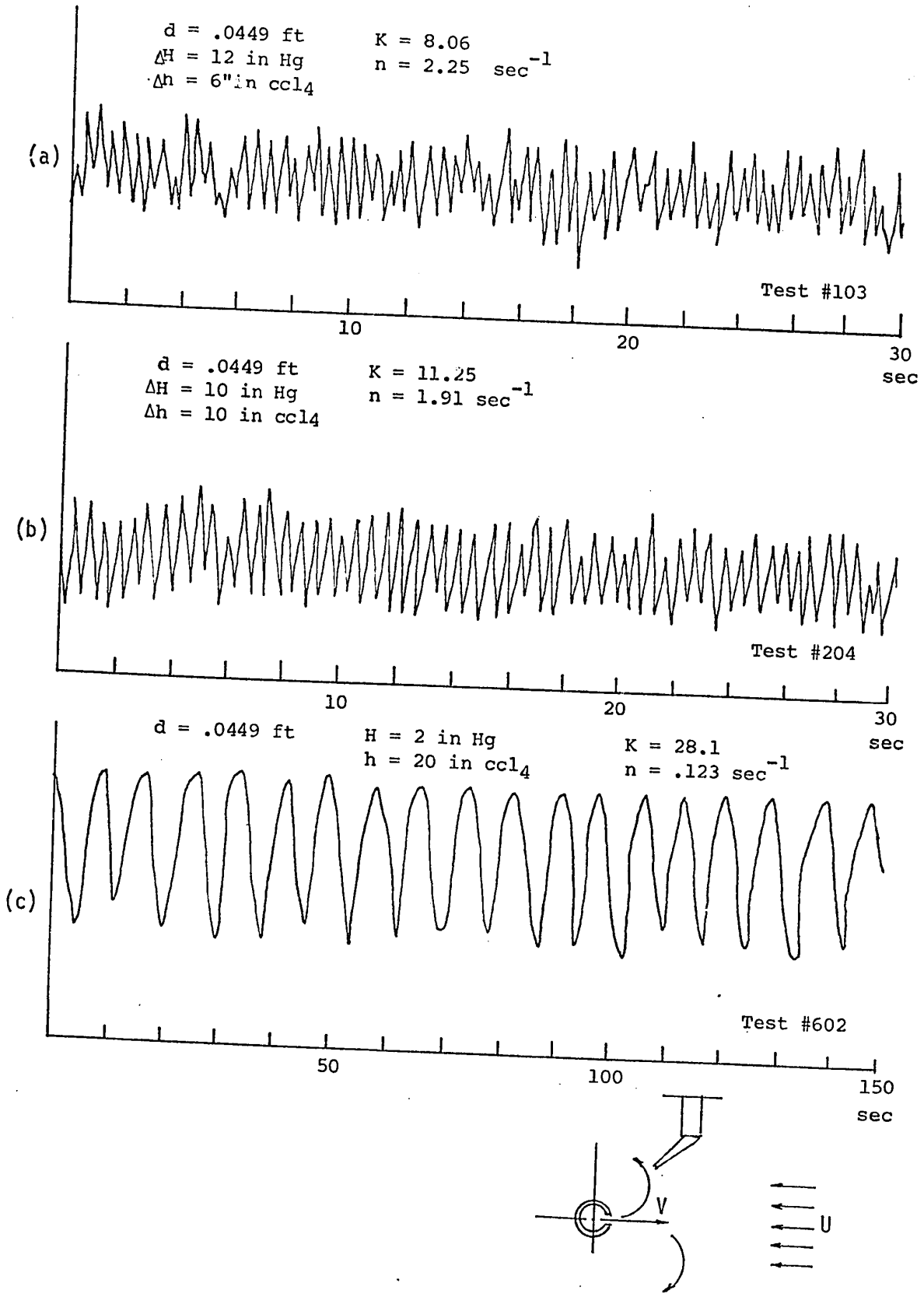

FIGURE 23 VORTEX SHEDDING - JET ONLY

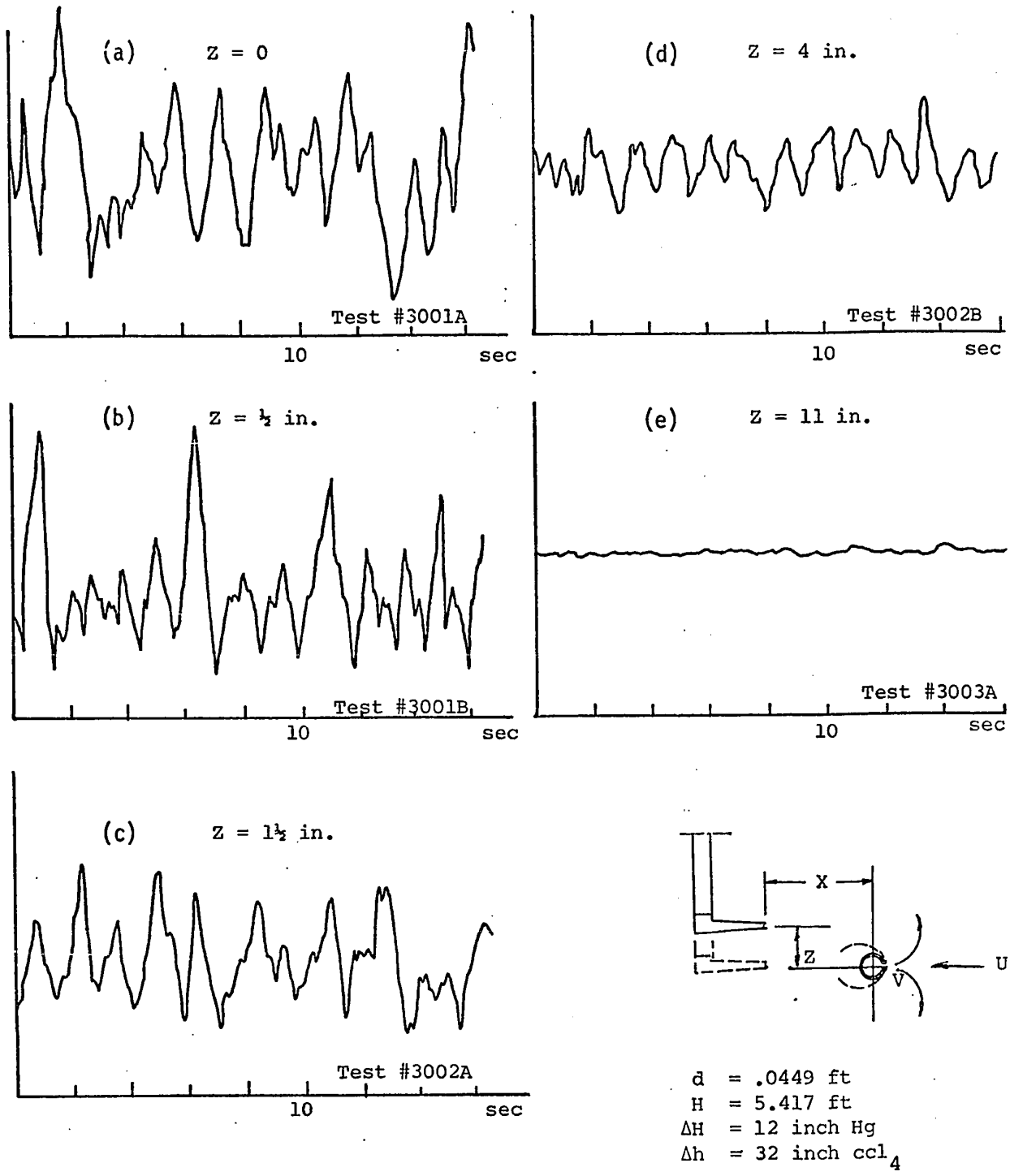

FIGURE 24 INTENSITY OF TURBULENCE IN THE WAKE

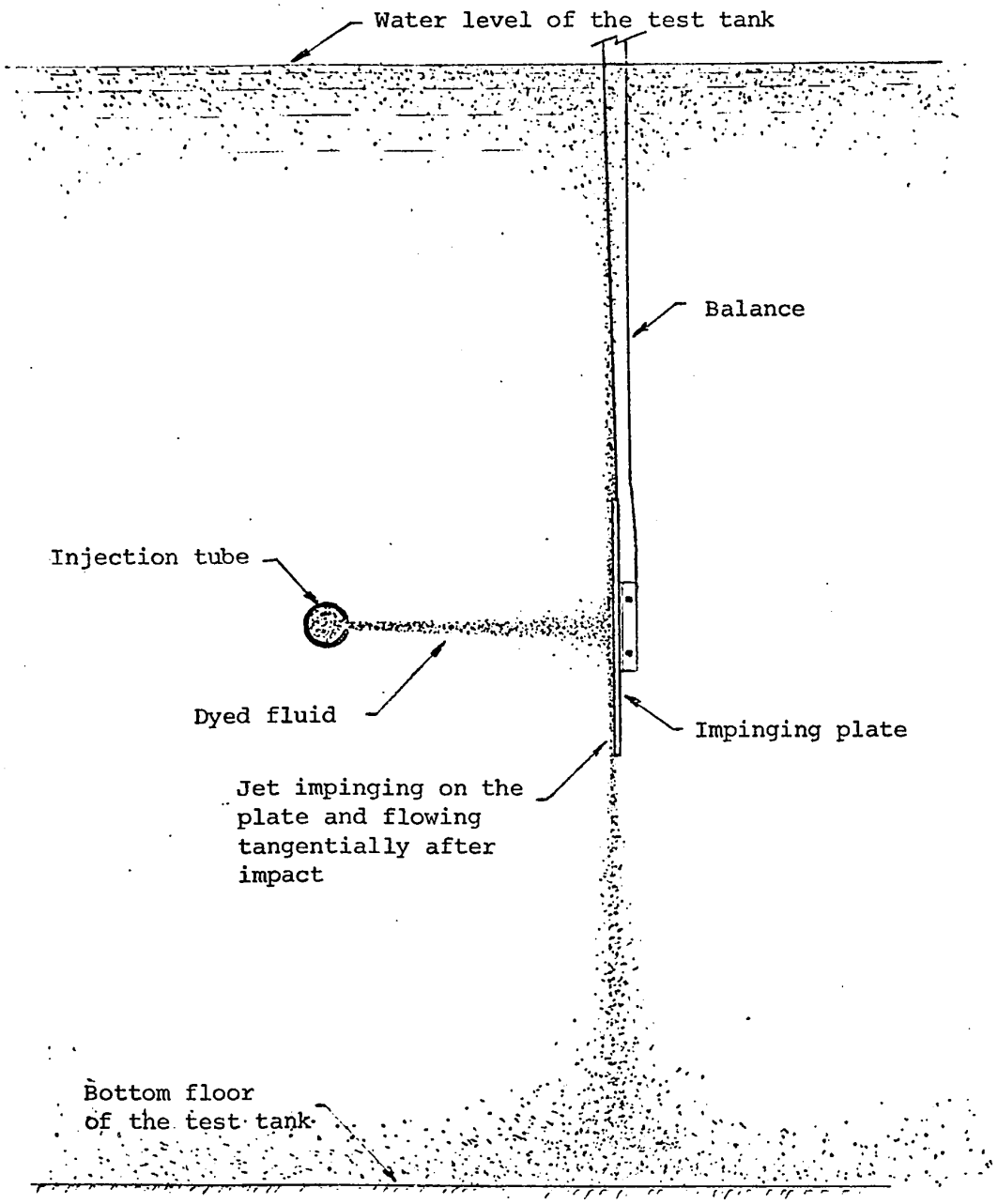

FIGURE 25 FLOW PATTERN OF JET IMPINGING ON PLATE

BIBLIOGRAPHY

1. Robillard, Luc : "Periodic Motion of A Two Dimensional Plane Jet In A Counterflow" Project No. NRC-A-4197 September 1969

2. Hopkins, D.F. : "A Study of Fluid Jet Penetration" Ph. D Thesis, Mechanical Engineering Dept., Univ. of Illinois, 1962

3. Strouhal, V.: Ann. hys. Und Chemie. New Series Vol. 5, P. 216-251

4. Roshko, A. : "One The Development of Turbulent Wakes From Vortes Streets" NACA Rep. 1191, 1954

5. Rao, T.R.K. "Investigation of The Penetration of A Jet Into A Counterflow" Master's Thesis, Dept. of Mechanical and Hydr., University of Iowa, 1958

6. Ramamurthy, A.S. Robillard, L. Lin, T.C. : "Phénomènes de transfer dans le cas d'un jet a contre-courant" Proceedings IAHR Aug 1971, Vol. 1

7. Colin, P.E. : "The Wall-Jet Beneath A Counterflowing Stream" DAJA 3767-C0045, March 1968

8. Vallentine, H.R. : "Applied Hydrodynamics" New York Plenum Press, 1967

9. Rouse, H. : "Diffusion of Submerged Jets" TASCE Vol. 115, P. 639, 1950

10. Schlichting, H. : "Boundary Layer Theory" McGraw-Hill, New York, 1968

BIBLIOGRAPHY (cont'd)

11. Daily, J.W. & Harleman, D.R.F. : "Fluid Dynamics" Addison-Wesley, 1966

12. Ramamurthy, A.S. Robillard, L. Duong, V.L., & Bhaskaran, P. : "Unstable Characteristics of A Plane Counterjet" CanCam Calgary Proceedings, May 1971

13. Ramamurthy, A.S. & Robillard, L. "Counter Jet Flow Characteristics Including Blockage Effects" to be published.

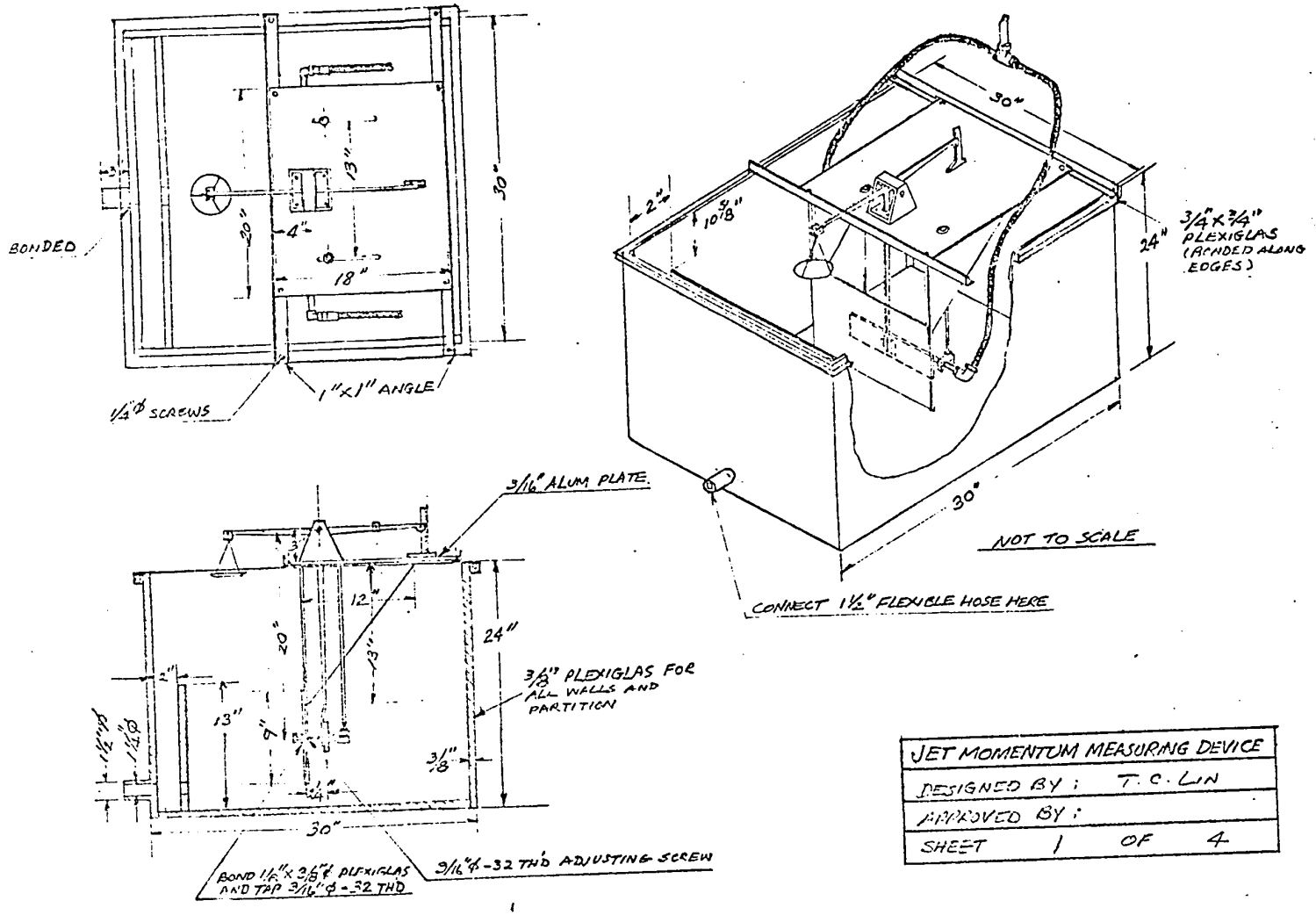

JET MOMENTUM MEASURING DEVICE			
DESIGNED BY:	T. C. LIN		
APPROVED BY:			
SHEET	1	OF	4

APPENDIX 1 DETAILED DESIGN OF THE BALANCE

APPENDIX 1 (CONT'D)

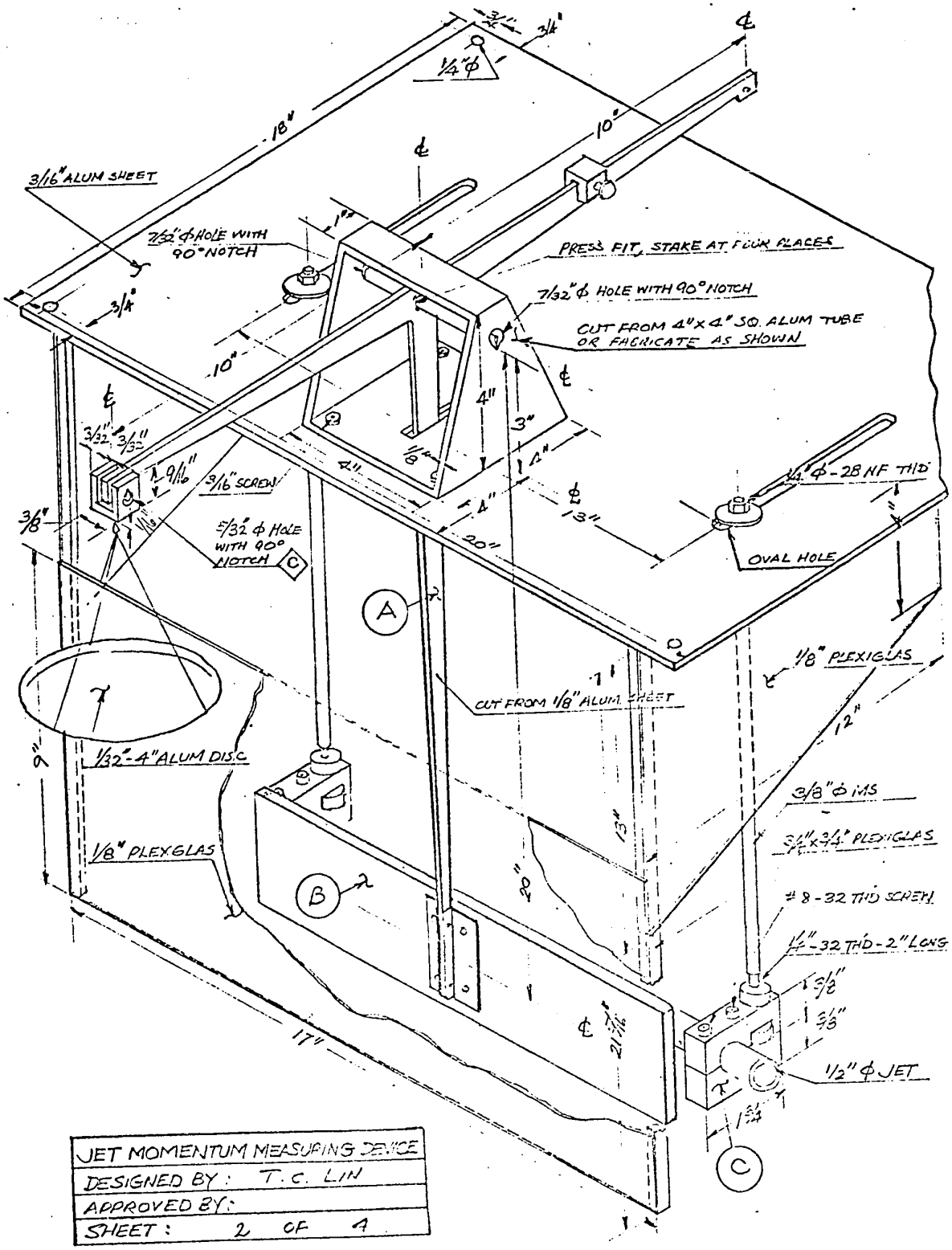

APPENDIX 1 (CONT'D)

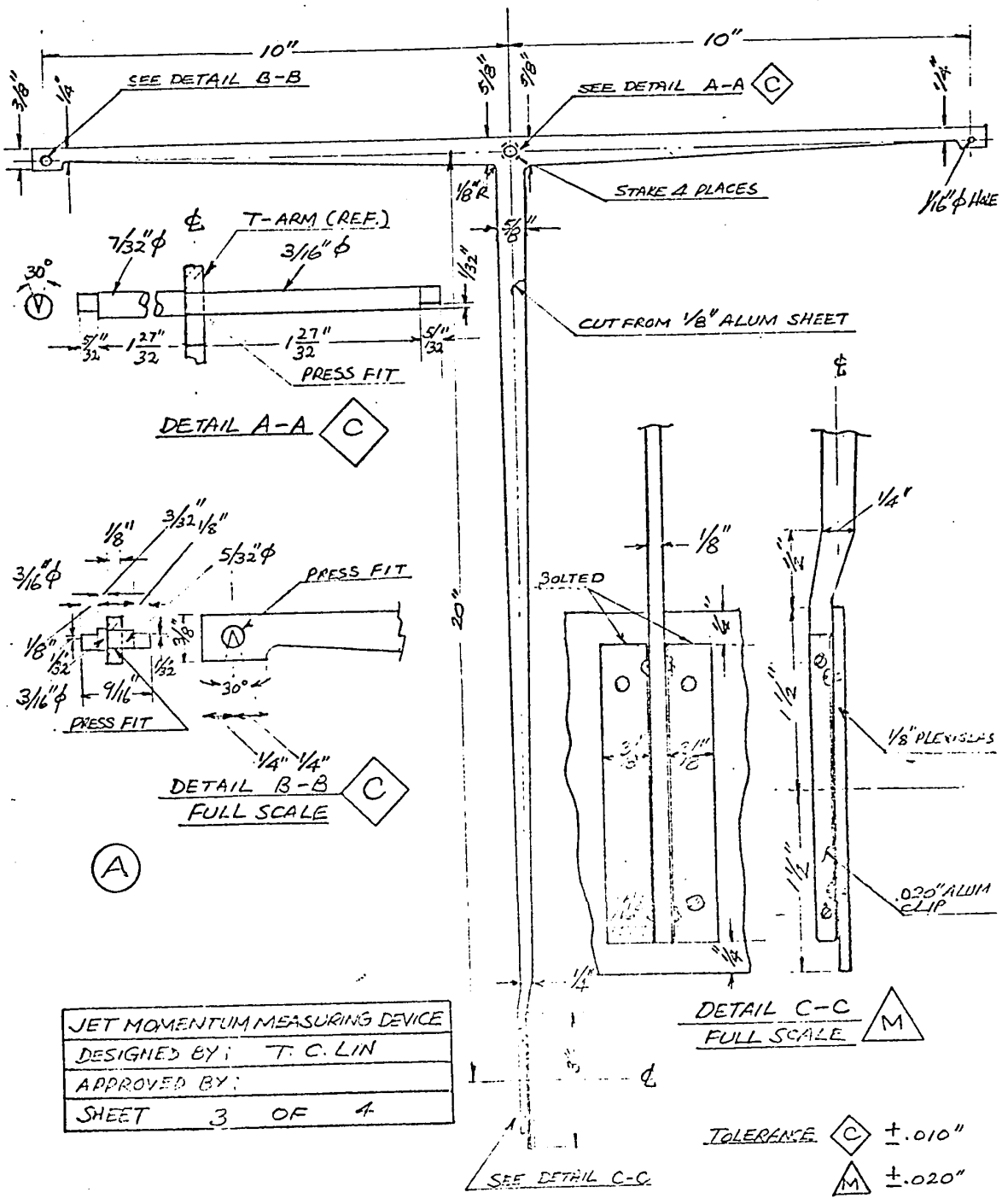

JET MOMENTUM MEASURING DEVICE
DESIGNED BY: T. C. LIN
APPROVED BY:
SHEET 3 OF 4

APPENDIX 1 (CONT'D)

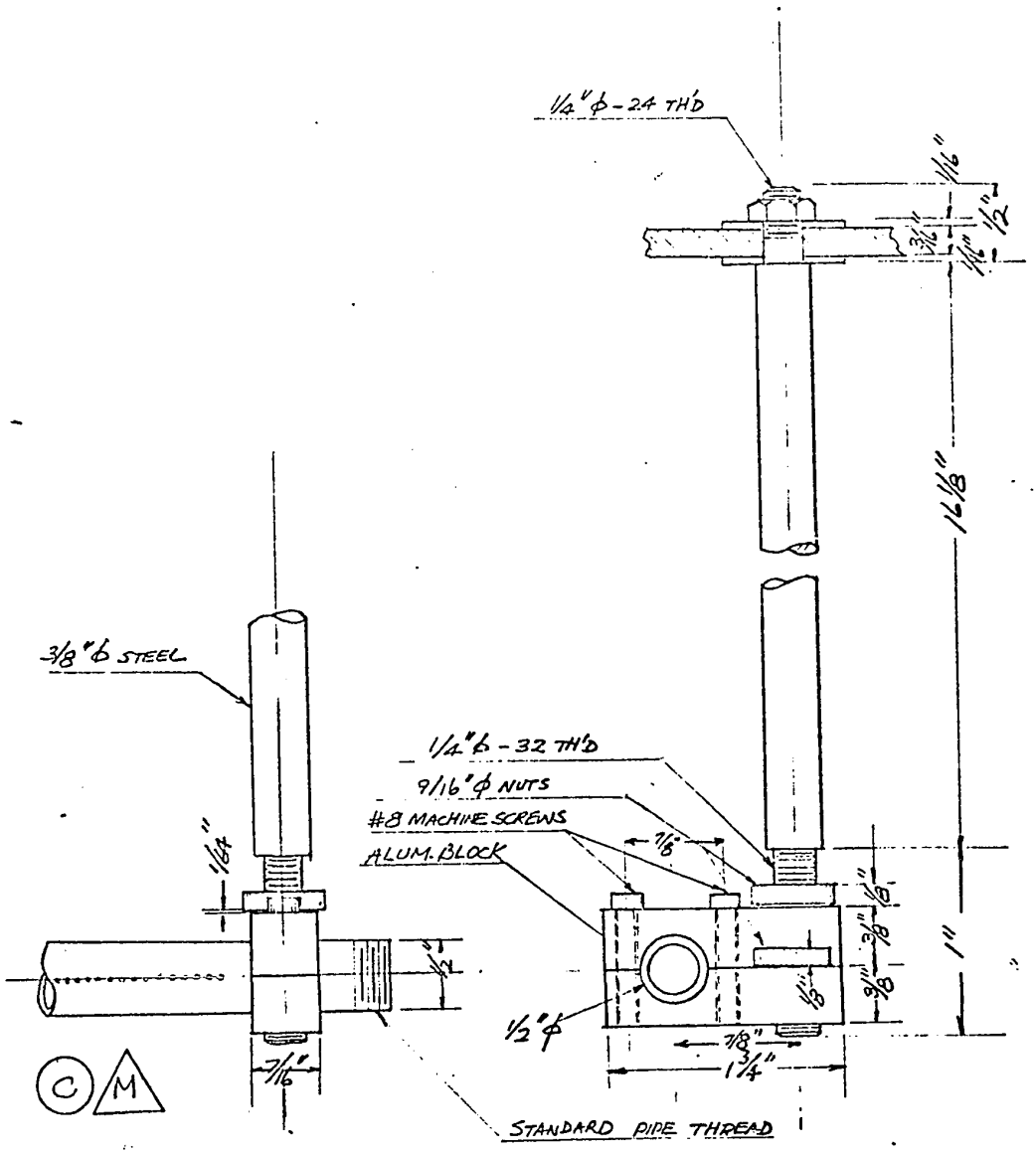

JET MOMENTUM MEASURING DEVICE
DESIGNED BY: T. C. LIN
APPROVED BY:
SHEET 4 OF 4

APPENDIX 2 SOME CALCULATIONS

(1) Reference: Eqn (4)

d, diameter of jet injection device = .0449 ft

S, Strouhal number = .21, when R>1200

$$U = \frac{n\,d}{S} = \frac{.0449n}{.21} = 0.214\ n \quad \text{ft/sec}$$

From Table 1,

$$n = 3.60 \qquad U_{cal} = 0.214 \times 3.6 = .770 \text{ ft/sec}$$

(2) Reference: Table 2

wt = 20 lbs.

T = 95.25 sec

$$Q_j = \frac{wt}{T} = \frac{20}{95.25} + .2099 \text{ lb/sec}$$

$$= \frac{.2099}{62.4} = .003356 \text{ ft}^3/\text{sec}$$

(3) Reference: Table 3

$$Q_j = .00851 \text{ ft}^3/\text{sec} \qquad b = \frac{10}{12} \text{ ft}$$

$$wt = 355.27 \text{ gram} = \frac{355.27}{453} = .784 \text{ lb.}$$

$$F = \frac{wt}{2} = .392 \text{ lb.}$$

$$J = F/\rho b = \frac{.392}{1.939\ b} = .2423 \text{ ft}^3/\text{sec}^2$$

(4) Reference: Eqn (11)

$$F = \rho \int_{\infty} 2g\ (R - R_s)\ \text{Sin}\theta\ b\ dz$$

$$= 2\ \rho g\ b\ \text{Sin}\theta \sum_{z} (R - R_s)\ \Delta z$$

From Table 4,

$$(R - R_s)\ z = 17.905 \text{ cm}^2$$

$$\text{Sin} = \frac{2}{\sqrt{(10^2 + 2^2)}} = .194$$

Thus, $F = 2 \times 1.939 \times 32.2 \times .833 \times .194 \times 17.905 \times 3.281^2 \times 10^{-4}$

$= .389$ lbs.

(5) Reference: Table 5

From Eqn (12)

$$J_u = A \frac{\overline{V}^2}{b} = A \frac{(Q_j/A)^2}{b} = \frac{1}{bA} Q_j^2$$

$$A = 80 \times \pi \times (\frac{.033}{12X2}) = .000475 \text{ ft}^2$$

$$b = \frac{10}{12} \text{ ft}$$

Thus, $J_u = \frac{1.2Q_j^2}{.000475} = 2525.47\ Q_j^2$

(6) Reference: Table 6

$U = .856$ ft/sec

$J = .0112$ ft^3/sec^2

$n = 3.5$ sec^{-1}

$H = 5.417$ ft

$d = 0.449$ ft

$\nu = 10.9 \times 10^{-6}$ ft^2/sec

Thus, $S_s = \frac{J\,n}{U^3} = \frac{.0112 \times 3.5}{.856^3} = .0625$

$B = \frac{J}{U^2 H} = \frac{.0112}{.856^2 \times 5.417} = .0028$

$R_s = \frac{J}{\nu\, U} = \frac{.0112}{10.9 \times 10^{-6} \times .856} = 1.20 \times 10^3$

APPENDIX 3 SURFACE TENSION EFFECTS

A water jet discharging into air through a small orifice forms a tubular beam. By taking this tubular beam as a free body, one may draw a sketch as below. This water jet discharges horizontally and the force caused by the surface friction is assumed negligible.

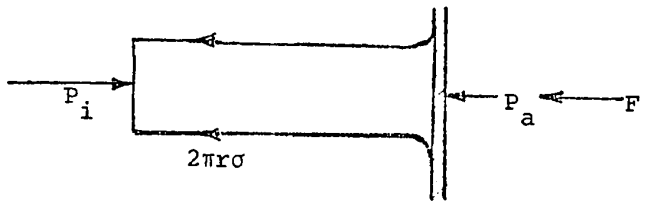

Let r = radius of the tubular beam †

p_i = pressure inside the beam

p_a = atmospheric pressure

σ = surface tension

Since ΣF_x = Change in Momentum

$$\therefore \quad p_i \pi r^2 - p_a \pi r^2 - 2\pi r\sigma = -\int_o^r \rho (v_r \, 2\pi r \, dr) \, v_r$$

$$= -\int_o^r \rho v_r^2 \, 2\pi r \, dr$$

The resulting force acting on the plate measured by the balance is therefore equal to

$$F = -(P_i - P_a) = -(p_i - p_a)\pi r^2$$

$$= \int_o^r \rho v_r^2 \, 2\pi r \, dr - 2\pi r\sigma$$

With the same pressure differential the measured force is always less than the actual momentum whenever surface tension exists.

† correction may be required on the radius of the tubular beam, which may not be the same radius of the orifice due to contraction effect.